nature communications

Article

https://doi.org/10.1038/s41467-025-61464-z

Neurophysiological evidence of human hippocampal longitudinal differentiation in associative memory

Received: 22 August 2024

Accepted: 20 June 2025

Published online: 25 July 2025

Check for updates

Tung V. To[1], David X. Wang[1], Cody B. Wolfe[1] & Bradley C. Lega[1,2]

In humans, the hippocampus exhibits evident structural and connectivity differences along the longitudinal axis. Experiments in rodents and more recently in human subjects have stimulated several theories of functional longitudinal specialization. This question pertains directly to the management of neurosurgical patients, as nascent technologies permit more precise treatments that can selectively spare longitudinal regions. With this in mind, we investigated hippocampal longitudinal specialization in 32 human intracranial EEG subjects as they performed an associative recognition episodic memory task. Utilizing the behavioral contrasts available in this task, we characterize the neurophysiological features that distinguish the anterior versus posterior hippocampal activity during recollection and familiarity–based memory retrieval, as well as novelty processing. We use subspace representations to characterize longitudinal differences in the temporal dynamics of key computational processes ascribed to the hippocampus, namely pattern separation and pattern completion. We place our findings in the context of existing models, adding to sparse literature using direct brain recordings to explicate the functional differentiation along the hippocampal longitudinal axis in humans.

Episodic memory requires the formation of novel associations between item and context, which makes strict demands on the hippocampal formation[1,2]. The hippocampus exhibits obvious anatomical differences, including alterations in the relative composition of CA1 vs CA3/Dentate Gyrus (DG) along the longitudinal axis[3–5]. Further, the anterior and posterior hippocampus participate in different connectivity networks. Several studies have anatomically characterized these distinct circuits, using methods such as animal tracer studies[6,7], as well as human dissection and tractography[8–10]. These segments communicate with the cortex through the medial/intermediate and lateral bands of the entorhinal cortex (ERC), respectively, which are only sparsely interconnected in tracer studies[11]. Standard and high-resolution fMRI data in humans have shown significant association between anterior hippocampus (AH) and perirhinal cortex (PRC), and posterior hippocampus (PH) and parahippocampus[12,13]. There is also evidence to correlate AH with a number of regions including amygdala and anterolateral temporal lobes, and PH with anterior and posterior cingulate cortex[14]. Drawing upon these disparate lines of evidence, investigators have proposed several models of anterior versus posterior hippocampal differences. Some examples within this menagerie include encoding vs. retrieval differences in longitudinal activation (HERNET model), spatial (PH) vs non–spatial (AH) representations, and affective (AH) vs non–affective (PH) memory processing[14–17]. More recently, Poppenk proposed a nuanced model in which the key difference is in the level of granularity of information processing (more precise in the posterior hippocampus), termed gist/detail models[18]. This model is supported by the well–known finding that the specificity of place fields progressively change along the axis in rodents[19]. Strange then proposed a related model by which this difference in representational specificity leads to an association of AH with semantic

[1]Department of Neurological Surgery, UT Southwestern Medical Center, Dallas, TX, USA. [2]O'Donnell Brain Institute, UT Southwestern Medical Center, Dallas, TX, USA. e-mail: bradley.lega@utsouthwestern.edu

integration of episodic information[20]. Potential cognitive differences in processing novel items have been reported since the early days of episodic memory experiments[21–23]. However, the precise neurophysiological mechanism that supports this cognition has not been characterized by using direct brain recordings, especially as it pertains to models of anterior/posterior hippocampal specialization[24].

Human electrophysiological studies have not directly supported these models. Namely, recordings from human intracranial EEG subjects performing spatial memory paradigms suggest there is commensurate size of place fields during virtual navigation experiments rather than a continuum of spatial specificity (this is also true in non–human primates)[25,26]. Likewise, published work identifying time–sensitive cell populations (temporal analogs of place cells) in the human hippocampus failed to reveal longitudinal differences in time field width[27]. More generally, robust activity of AH in human iEEG subjects (analogous to ventral in rodents) during episodic paradigms without emotional content suggests that accounts predicated on emotional vs. non–emotional memories are at best incomplete[28], although gene expression profiling[29] and connectivity information suggest that AH has an association with affective processing within the wider context of memory encoding.

This is not to say that no electrophysiological evidence of longitudinal differentiation exists. Costa[30] reported enhanced AH oscillatory activity during emotional memory processing, consistent with the affective model proposed by the Mosers[31] and the gene expression study by Ayhan et al.[29]. During spatial navigation tasks, iEEG data have supported existence of traveling wave events along with the hippocampal axis, with the preferred direction predictive of memory performance[32]. In subjects performing free recall, our group previously reported relatively greater posterior hippocampal theta oscillatory power during encoding, with evidence of posterior-to-anterior traveling wave activity[33]. Of note, these theta oscillations appear to be sensitive to cholinergic manipulation[34]. However, this longitudinal asymmetry in theta oscillations is not universal across episodic memory paradigms. In associative memory experiments, relatively commensurate anterior/posterior theta and gamma activity has been reported, echoed in non–invasive data[28,35]. Theta oscillations provide a lens through which to understand anterior/posterior differentiation because of their importance to episodic processing[36,37]. Theta oscillations underlie key features of memory including item/context binding, sequence generation, and context recovery[38–40]. Physiologically, theta oscillations are essential by permitting precisely–timed convergence of activity[41,42]. Differences in theta oscillatory activity, including amplitude, connectivity, cross–frequency coupling, and center frequency have been reported along the hippocampal axis during episodic memory processing and spatial navigation[28,43–45].

This paper examines the complementary processes of pattern separation and pattern completion through the lens of the behavioral contrasts constructed in the AR task. Pattern separation, a critical process in episodic memory, allows the hippocampus to encode overlapping sensory inputs as distinct representations, thereby preventing interference among similar memories (see[46] for review). This process involves the DG, which transforms input from ERC into orthogonalized signals relayed to CA3, facilitate memory encoding and retrieval[47]. Conversely, pattern completion enables the recall of entire memories from partial cues. Previous work in humans has suggested that these two complementary processes modulate the activity along hippocampal longitudinal axis, driven by the anatomical division of connectivity with cortical and subcortical networks[18,48,49]. Additionally, the quality of the cues themselves may modulate longitudinal activation in separation and completion; a highly preserved, detailed cue may engage the PH directly to pattern complete during recollection, while a cue with low integrity or is highly based on schemas may be activate vmPFC and AH connections to generate a 'gist'-like representation to pattern complete[49]. These processes have commonly been studied using the mnemonic similarity task (MST)[50], thus by implementing the AR task, we can evaluate whether similar mechanisms are engaged across varying stimuli and paradigms.

To further investigate human hippocampal longitudinal differentiation, we examined intracranial recordings performed as subjects engaged in an associative recognition memory task. Along with differentiating familiarity versus recollection–based memory representations, associative recognition operationalizes contrasts between correctly identified novel items (novelty processing) and associative misses, i.e., previously seen 'intact' items identified as 'rearranged' (recalled on the basis of familiarity; associative information was lost). Previous investigations using non–invasive imaging have established the utility of this contrast to identify novelty–related processing networks in humans[51]. Focusing on hippocampal theta oscillations, we used the set of contrasts available in the AR paradigm to investigate longitudinal specialization. Additionally, we tested whether electrodes precisely localized to distinct hippocampal subregions, namely CA3 vs. CA1, exhibit differences in associative item processing. We then sought to investigate longitudinal differences in the key computational processes of pattern separation and pattern completion, operationalized during the encoding and retrieval of associative hits within the AR paradigm, by characterizing the temporal dynamics of low-dimensional representations of individual associates. By selecting the appropriate behavioral contrasts in AR, we believe these stimuli can be analogous to MST paradigms that are often used to investigate pattern separation and completion[50,52]. Responses of intact, new, and rearranged items (respectively, see Behavioral Task) pose similar challenges to the memory system in terms of distinguishing overlapping representations. In all of these analyses, we used an unprecedented dataset of longitudinal recordings, providing the spatial and temporal resolution necessary to resolve these key questions.

Results

Intracranial EEG data from 32 epilepsy patients were analyzed for this study, summarized in Table 1. These electrodes are also mapped onto and visualized using BrainNet Viewer. We confirmed the separate anterior vs posterior location of electrodes via expert neuroradiological review of post–implant imaging, and note that at our center (as with most high-volume sEEG institutions) hippocampal targeting incorporates laterally inserted anterior and posterior recordings routinely with specific targeting based on anatomical features (uncal notch).

Behavioral Results

Subjects completed an average of 277 items (SD of 101; see Table 2) retrieval items throughout each experimental session. We excluded subjects who did not meet the a priori defined inclusion criterion of achieving a probability of recollection ($pR > 0$). Median response times for Intact-Intact items were 432 ms, Intact-Rearranged were 597 ms and Novel-Novel items were 502 ms, shown in Fig. 1. Among the three types of items shown at retrieval, patients had a similar fraction of response and no-response; median response rates were 88.9% for 'Intact,' 91.1% for 'Rearranged,' and 92.9% for 'Novel' items. The fraction of correct item responses, shown in Table 2 match previously published results in human intracranial EEG[28,53]. Behavioral performance in this patient cohort is consistent with previous reports for associative recognition in surgical epilepsy patients[28]. This task places explicit demands on the hippocampal memory system to disambiguate items recovered on the basis of familiarity versus recollection. This reduces recall fraction, but also elicits consistent hippocampal activation[54].

Longitudinal differences in theta power modulation during recollection

We tested hypotheses motivated by existing models of hippocampal longitudinal specialization. We predicted that the PH would exhibit

Table 1 | Patient demographic information

ID	Sex	Hemisphere	Location	Duration (years)	Onset (years)	Handedness	# Electrodes
1	M	Left	Pre-motor area	20	2	R	2
2	M	Left	L intraparietal sulcus, L medial temporal gyrus	24	10	R	16
3	F	Left	L fusiform gyrus	9	13	R	21
4	F	Right	R anterior cingulate/SFG prefrontal, R anterior insula/frontal operculum	19	17	R	15
5	M	Bilateral	L hippocampus and amygdala, and R insula	28	11	R	12
6	M	Right	STS/MTG posterior	19	25	L	20
7	M	Right	R temporal lobe	2	24	R	27
8	M	Left	L supplementary motor area	5	15	R	3
9	M	Bilateral	R temporal lobe and L hippocampus	3	19	R	15
10	F	Left	L posterior insula	8	36	R	18
11	M	Bilateral	Bi-temporal; L and R separately	11	20	L	19
12	M	Right	R hippocampus, R temporal	8	36	R	20
13	M	Right	R hippocampus	27	4	R	22
14	F	Left	L entorhinal	4	50	L	15
15	F	Left	L hippocampus and temporal pole	4	33	R	12
16	F	Left	L anterior hippocampus and amygdala	10	21	R	17
17	M	Right	Pre-frontal/pre-motor of R SFG & MFG	6	17	R	15
18	M	Right	R hippocampus	11	34	R	7
19	M	Right	R temporal	4	39	L	28
20	F	Left	Anterior schizencephalic cleft	23	22	L	11
21	M	Right	R MTG, right SMG/angular gyrus	20	30	R	22
22	F	Left	L hippocampus	10	16	R	6
23	F	Bilateral	L hippocampus, right fusiform gyrus	5	19	L	1
24	M	Right	R hippocampus	2	29	R	5
25	M	Right	R temporal regions	26	30	R	20
26	F	Left	L posterior insula, left temporal operculum	9	15	R	8
27	F	Right	R posterior hippocampus	8	25	R	16
28	F	Left	L hippocampus	47	3	R	10
29	F	Bilateral	L hippocampus, right hippocampus	21	18	R	26
30	F	Left	L hippocampus	17	35	R	21
31	M	Right	R SFG/MFG	10	24	R	7
32	F	Right	R hippocampus	2	41	R	6

Age of patients ($n = 32$) ranges from 20 to 56, with a mean of 36 and standard deviation of 11.

Table 2 | Mean fraction of patient responses to Intact, Rearranged, and New items shown during retrieval

Item Presentation	Patient Response		
	Intact mean (std)	Rearranged mean (std)	New mean (std)
Intact	**0.467 (0.237)**	0.175 (0.125)	0.147 (0.120)
Rearranged	0.307 (0.177)	**0.284 (0.200)**	0.202 (0.144)
New	0.145 (0.112)	0.213 (0.152)	**0.435 (0.221)**

Summary statistics were derived from 51 patients involved in this study, with bold values denoting correct judgments. Patients were shown an average of 277 items (S.D. = 101; some patients participated in multiple sessions), responded to an average of 223 items (S.D. = 110), and correctly responded to an average of 116 items (S.D. = 62). Mean and standard deviation of correct response fraction = 0.4127 (0.1721). Correct judgments (bolded values) are denoted by associative hits ('Intact' response to an intact pair shown at retrieval), associative correct rejections ('Rearranged' response to a rearranged pair), or correct rejections ('New' response to a new item). Associative misses are denoted as a 'Rearranged' response to an originally intact item.

relatively greater oscillatory power during successful recollection by analogy from models that posit greater detail and specificity of representations in dorsal areas[19]. By contrast, we predicted that successfully recognized novel items would exhibit greater activity in AH, building on similarities in the processing of novel and salient images in rodent experiments and non–invasive studies[55]. For items retrieved on the basis of familiarity, by contrast, we predicted relatively greater AH activity.

We used functional comparisons previously established for behavioral contrasts within the associative recognition paradigm[51]. Namely, recollection effects were assessed by contrasting associative hits with associative misses, and novelty–related processing was assayed by contrasting neurophysiological activity during correct rejections (successfully identified novel items) with associative misses (i.e., items recovered on the basis of familiarity)[28,51,54]. We focused our analysis on theta activity given its well–established importance in memory processing and previous evidence of longitudinal differences in theta power changes during mnemonic processing[28,33].

Normalized power recorded separately from AH and PH was plotted for the entire time-frequency space. Figure 2 shows these data for the three conditions assayed within the associative recognition paradigm. Recollection–related contrasts revealed expected power increases across the theta frequency band during the processing of associative hits (mixed-effects model, FDR corrected $p < 0.05$). Interaction models revealed recollection effects in the theta band that were greater in the posterior hippocampus centered around 4 Hz most evident between 600 and 1200 ms. Specifically, these recollection

https://doi.org/10.1038/s41467-025-61464-z

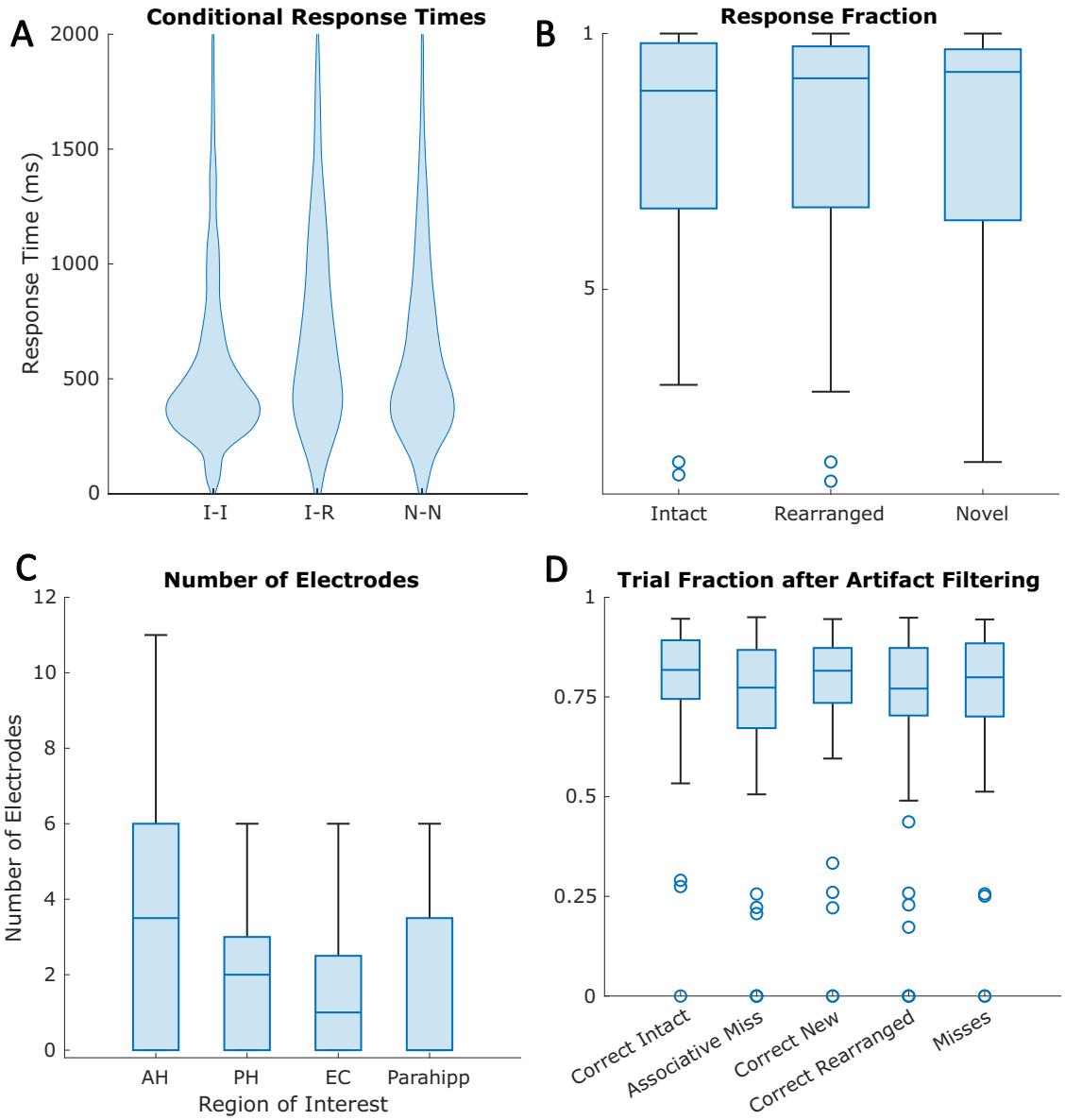

Fig. 1 | Summary of the dataset. A Average word pair response times for associative hits, misses, and novel items. Box plots in *A*, *B*, and *C* show the median (center line), interquartile range (box), and the whiskers represent the range within 1.5× IQR from the lower and upper quartiles. Points beyond this are plotted as outliers. **B** The proportion of trials with subject responses for each item type ($N = 67$ per response type). **C** Median number of electrodes in region of interest per patient ($N = 32$ patients per region). Anterior hippocampus (AH): 3.5 (IQR 6), posterior hippocampus (PH): 2 (IQR 3), entorrhinal cortex (EC): 1 (IQR 2.5), and parahippocampus (Parahipp): 0 (IQR 3.5). **D** Fraction of trials remaining after artifact filtering during our EEG pre-processing step ($N = 67$ electrodes per condition). All items shown had a median fraction between 0.75 and 0.85, without clear significance between trial types.

effects are more evident in slow theta, as the pattern observed in the fast theta frequency band are more ambiguous (2B). For rigor, we used also tested our results using a convergent statistical method based permutation testing, shown in the supplementary (Supplemental Fig. 1). We confirmed that the functional and longitudinal differences described above were significant as random effects in this model.

Items recovered via familiarity, by contrast, only exhibited theta power differences late in the time series, nearly 1500 msec after item onset. However, these familiarity–based effects were significantly stronger in the AH than PH across the broad theta frequency range (Fig. 2A interaction plots). These results were broadly similar across both statistical methods, with greater fast theta power for familiar items late in the time series.

To test for longitudinal differences during the correct identification of novel items, we first determined that we observed novelty–related theta power changes, defined as the increase in novel pair power compared to associative misses for each region: $NN > IR|AH$, $NN > IR|PH$. As depicted in Fig. 2, slow theta (2–5 Hz) oscillations exhibited significant novelty effects from 1000 to 1500 ms for AH more than PH. The regional interaction of these two comparisons showed an area overlapping with the primary effect of novel items (greater theta power in AH). The novelty–related power increases, and the interaction term describing longitudinal differences, were not observed in the fast theta (5–9 Hz) frequency range.

Intrahippocampal Phase Synchrony

One of the hallmarks of successful item retrieval during episodic memory processing is enhanced intrahippocampal connectivity, especially in the theta frequency range. Our group and others have reported connectivity changes across the broad 2–10 Hz frequency band within the hippocampus[33,43,45], and we applied similar approaches to understand the temporal dynamics of hippocampal connectivity

https://doi.org/10.1038/s41467-025-61464-z

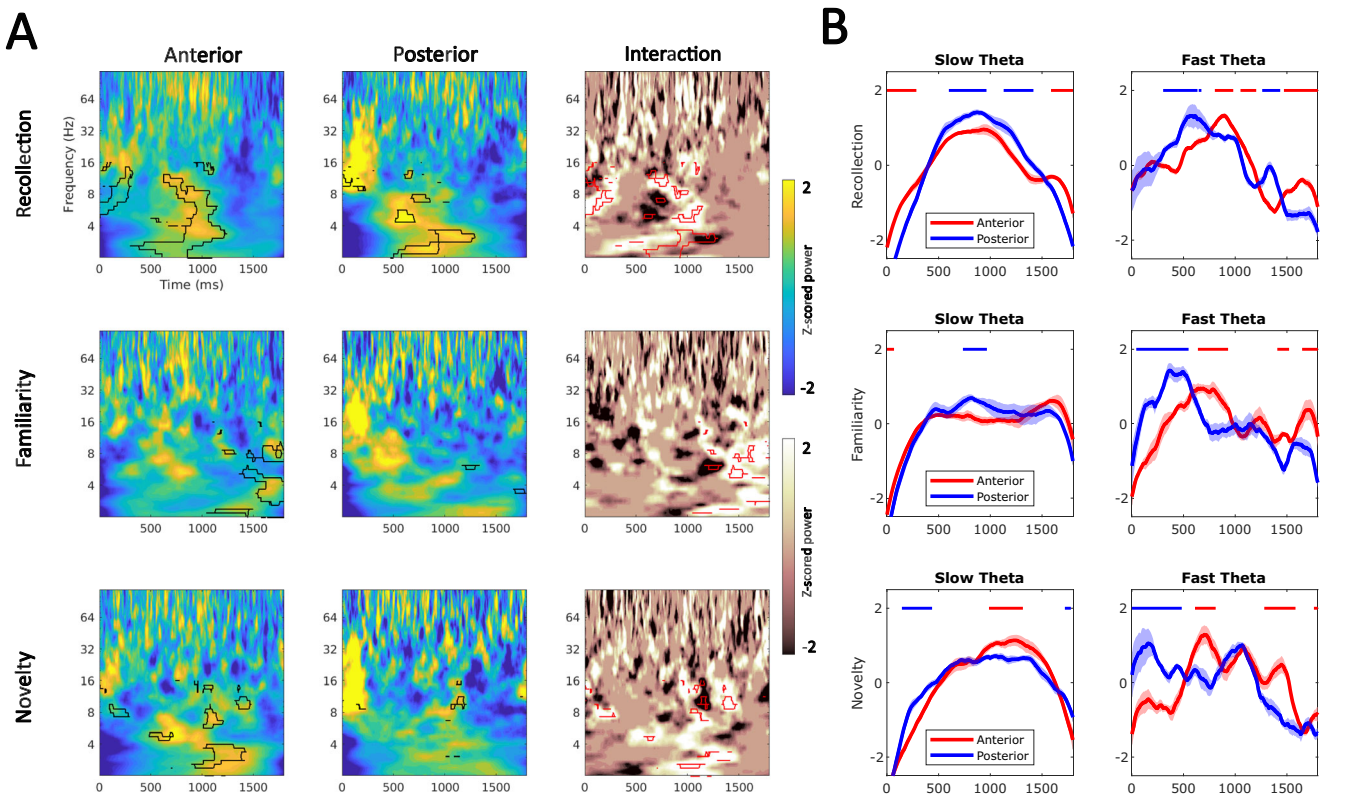

Fig. 2 | Hippocampal power differences during associative recognition. A Time-frequency plots depicting normalized power between anterior hippocampus (AH) and posterior hippocampus (PH) with interaction effects from model estimates. Recollection, familiarity, and novelty effects are represented with I-I, I-R, and N-N items, respectively. Highlighted regions in black are time-frequency points that significantly differ in the corresponding contrast (I-I > I-R for recollection, I-R > X-N (complete misses) for familiarity, and N-N > I-R for novelty) using LMEM with FDR correction. The highlighted red pixels in the interaction plots represent time-frequency points during which there is significant region-contrast interaction (FDR), while the colors represent the main regional contributions (i.e., dark areas represent posterior > anterior, while bright areas represent anterior > posterior). **B** Aggregation of normalized power (I-I for recollection, I-R for familiarity, N-N for novelty) in plot *A* across slow (2–5 Hz) and fast (5–9 Hz) theta. Standard errors of normalized power across electrodes are shown as shading bands surrounding each line, which represents data mean. Significant longitudinal differences for each contrast from *A* were highlighted for each band.

during the processing of novel items (using the same behavioral contrast as above). We characterized differences in intrahippocampal oscillatory synchrony across all three classes of items using equation (3) to obtain a Rayleigh's Z-statistic, which was balanced for unequal sample sizes. Recollection was associated with increased 2–5 Hz slow theta synchrony 1000–1500 msec after item onset (Fig. 3), consistent with previous reports. We also report significantly increased phase synchrony for pre-stimulus items within the recollection contrast. Fast theta (5–10 Hz) oscillations, by contrast did not exhibit significant synchrony changes that would predict recollection outcome. During successful recognition of novel items, we instead did not observe any elevation in synchrony, distinguishing novelty processing from recollection in spite of similarities in theta power changes.

Longitudinal differences in Pattern Separation and Pattern Completion

A central concept in computational models of hippocampal function is that the hippocampus directly supports pattern separation and completion of input sensory (and other modality) information from the cortex[46]. Within a source memory paradigm such as associative recognition, item encoding requires pattern separation to differentiate associated pairs from other items and previously stored representations that may overlap with activity linked with items at study[56]. By contrast, memory retrieval in such a paradigm requires pattern completion as test items activate previously stored representations (for successful associates). We examined pattern completion specifically for correct associative rejections (rearranged items successfully labeled as rearranged) by employing a 'recall to reject' framework for interpretation (see Discussion). Participants shown old items linked with a novel associative pair first recover the memory of each item separately and then render a judgment ('rearranged'). These items create a unique opportunity to examine pattern separation because of the ability to generate distinct similarity vectors for each of the two items (with encoding–related activity). Using this opportunity, we devised an analytical framework to examine the temporal dynamics of pattern completion through reinstatement of low dimensional projections of complex feature vectors to visualize and quantify reinstatement of encoding patterns within these feature vectors in low dimensional subspace representations.

Results of the pattern completion analysis are shown in Fig. 4 where the average distance in the principle-component space was plotted with respect to time. The temporal dynamics of pattern completion for AH and PH distance shown in Fig. 4E are significantly different (Two-sample F-test for variance, f-statistic: 2.6898, df1 = 103, df2 = 103, p-value = 9.01e-7). We interpret results of our analytical approach to provide evidence of the temporal dynamics of pattern completion processes, as divergence of the similarity vectors suggests when processing of the input stimulus (at test) had diverged into traces more similar to the input stimuli observed during study (i.e., completion of the pattern provided by the input stimulus), reflected in 4G. The green bars above the line plots denote epochs during which representational distance for R-R items were significantly greater/less

https://doi.org/10.1038/s41467-025-61464-z

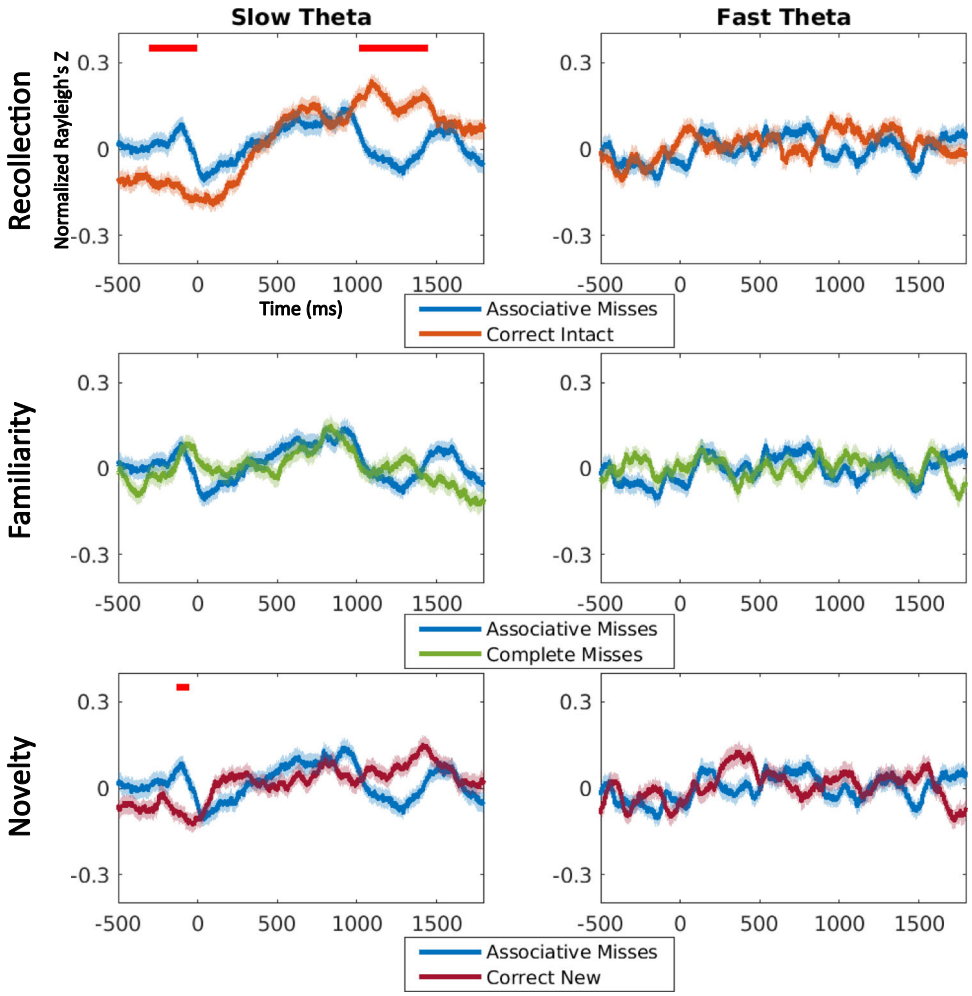

Fig. 3 | Phase synchrony along anterior-posterior hippocampus for each contrast, error bars represented SEM. Y-axis represents the normalized Rayleigh's Z, with corresponds to the degree of non-uniformity between anterior-posterior electrode pairs. Significant anterior-posterior synchrony differences that did not last for at least half a cycle of the respective bands (2–5 Hz for slow theta, 5–10 Hz for fast theta) were removed.

than the null distribution for each hippocampal subregion. The red bars above the plots denote epochs during which there was a significant longitudinal difference in these distances.

Based on these subspace representational analyses, pattern completion within AH peaks within 750 ms of stimulus onset, and again at 1250 ms, whereas in the posterior hippocampus pattern completion is most evident at 1000 ms and at 1500 ms following item onset at the time of test. Longitudinally, there are not many epochs during which the two regions show strong coupling, with A > P early on followed by a clear reversal of effects by 1000 ms, consistent with the temporal dynamics of theta power changes shown in 4F. The results provide neurophysiological correlates of hippocampal dynamics that underlie pattern completion along the hippocampal axis, providing temporally precise estimates of how recollection unfolds following a mnemonic stimulus. However, given the lack of clear differentiation in the magnitude of pattern completion between AH and PH, we do not interpret these data to suggest that longitudinal specialization clearly emerges when viewed through this (computational) lens.

We developed an approach to assay pattern separation using a similar subspace representational analysis in accordance with conceptions of pattern separation in associative paradigms. This utilized the set of vectors derived from hippocampal neural signals observed at the time of item encoding for all items, which we used as a distribution for comparison to vectors for individual items (see[57] for similar methods applied to item–specific activity vectors in a source paradigm). This method, in essence, tracks the distribution of all features of a single patient as it evolves along the time series, and notes the epoch, if any, that strays significantly from the distribution of features at the initial epoch, prior to any potential separation–related computation (distribution of a patient in 2-space shown in 5A). If the orthogonalization of these vectors during encoding truly supports the formation of associative memories, it is reasonable to expect that feature divergence during epochs that are unique to correct lure rejection over misses are detectable signals for pattern separation. For rigor, we also used a complementary method based upon the cosine distance of individual vectors, rather than the global distribution at each epoch, which takes into account the individual shift of vectors (distribution of a patient in 2-D space for 2 epochs in 5B). We reasoned that cosine distances should increase in time following item onset, and should (at minimum) distinguish successfully recollected items (I-I) from those that were completely forgotten or recovered on the basis of familiarity.

The results of the pattern separation analysis are shown in Fig. 5, where 5C shows the average fraction of trial distances that exceed the 90th percentile of distances for all epochs of a given patient. Trial distances were obtained by calculating the magnitude of feature vectors, and were tested across both conditions (correct and incorrect), as well as region (anterior and posterior). Using mixed-effects modeling with FDR correction (Q = 0.05), we found that there was a significant interaction between region (AH vs. PH) and condition (recall success)

https://doi.org/10.1038/s41467-025-61464-z

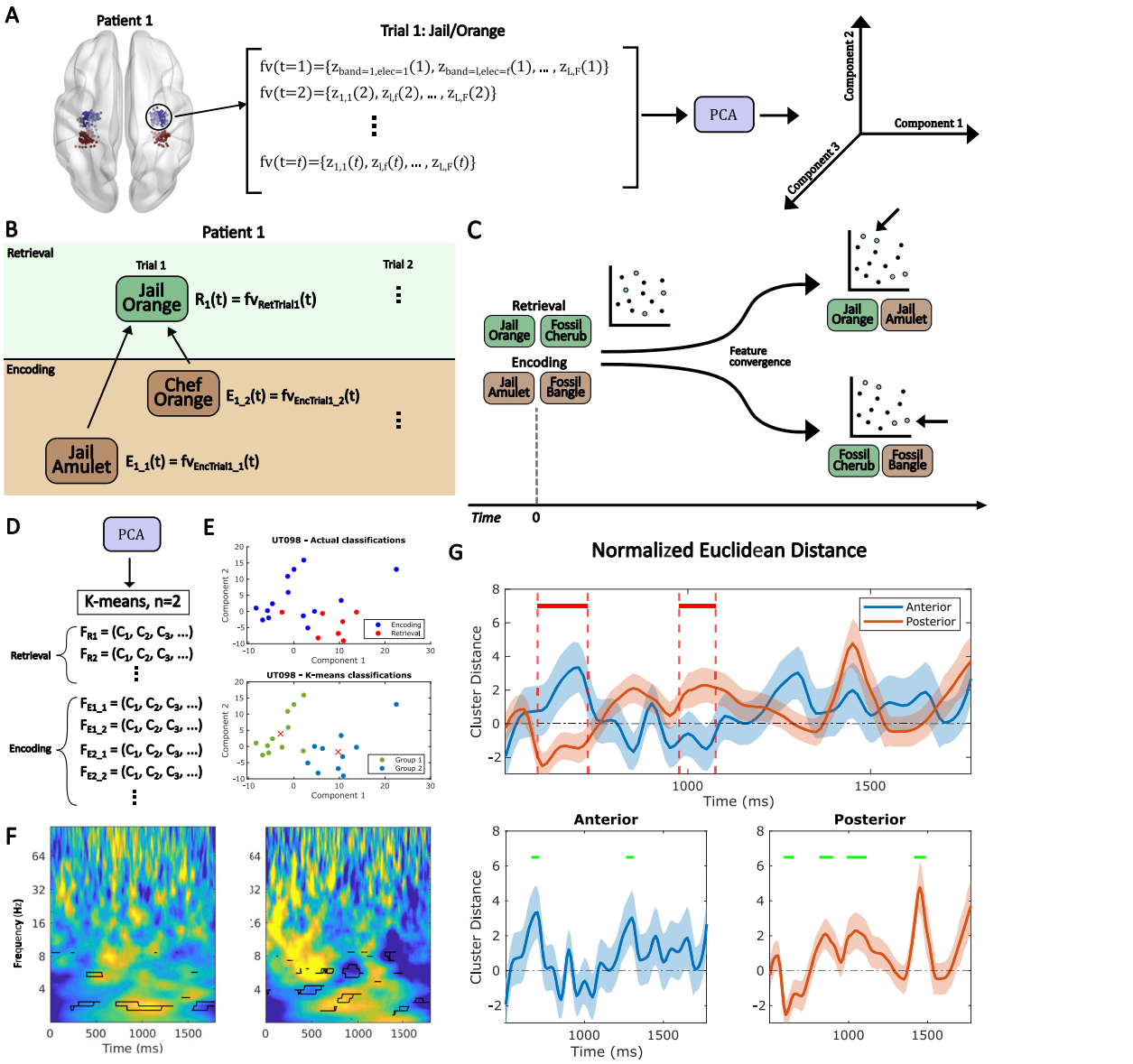

Fig. 4 | Subspace representational analysis of pattern completion. A Methods for feature vector generation from hippocampal electrodes, where features are generated from each band-electrode combination from each patient. Individual features are then normalized followed by PCA. **B** Trial selection process, where each word from an individual pair during encoding is matched to a correctly labeled rearranged pair during retrieval. **C** Conceptual diagram depicting time evolution of feature vectors for 2 encoding and retrieval trials of a given patient. **D**, **E** depicts k-means data frame construction and clustering for an example patient. **F** Normalized power spectrum for R-R items at retrieval for reference. Highlighted in black are pixels where RR > RI significantly for each region (with FDR correction). **G** Normalized Euclidean distance between centroids of k-means (k = 2) clustering when given encoding and retrieval trials of correctly rearranged (R-R) items. The data are represented by distance mean ± SEM. Distance was normalized to first 100 ms. Regions highlighted in red in the combined plot show significant longitudinal differences in distance (Two-sample Z-test from Z-scored centroid distance; $p < 0.05$, $N = 32$ patients for both groups), with cluster-based correction for multiple comparisons ($p < 0.05$ for at least 50 ms). The peaks highlighted in green in the individual plots below show completion distance that significantly diverged from baseline (cluster-based correction, $p < 0.05$ for at least 50 ms).

500 ms after item onset, where items that were later successfully recalled had a greater magnitude fraction in the AH than PH, as shown in red (5C). In other words, our results reveal evidence of distinct temporal dynamics characterizing hippocampal pattern separation across the hippocampus, with anterior hippocampal orthogonalization of input features earlier in time that predicts encoding success followed by maintenance of separated features from 400 to 550 ms following item presentation. Later in the time series, orthogonalization is significantly greater in the posterior hippocampus. These findings together characterize a 'bi-phasic' temporal dynamic underlying this critical process that unfolds along the hippocampal axis.

We observed similar results with our alternative method based on cosine distance, shown in 5D. For both correct and incorrect pairs, both AH and PH exhibited orthogonalization over time as the average distance approaches 1. However, through linear modeling and FDR correction, we found longitudinal differences unique to successfully recalled items that are stable through time, from 700 ms to 1200 ms, with evidence of greater orthogonalization in the AH (Fig. 5D). Later in time, orthogonalization in the posterior hippocampus increases but does not predict recall success. Overall, we interpret these data to reveal that both anterior and posterior hippocampus engage in pattern separation computation, however with distinct dynamics. They also

https://doi.org/10.1038/s41467-025-61464-z

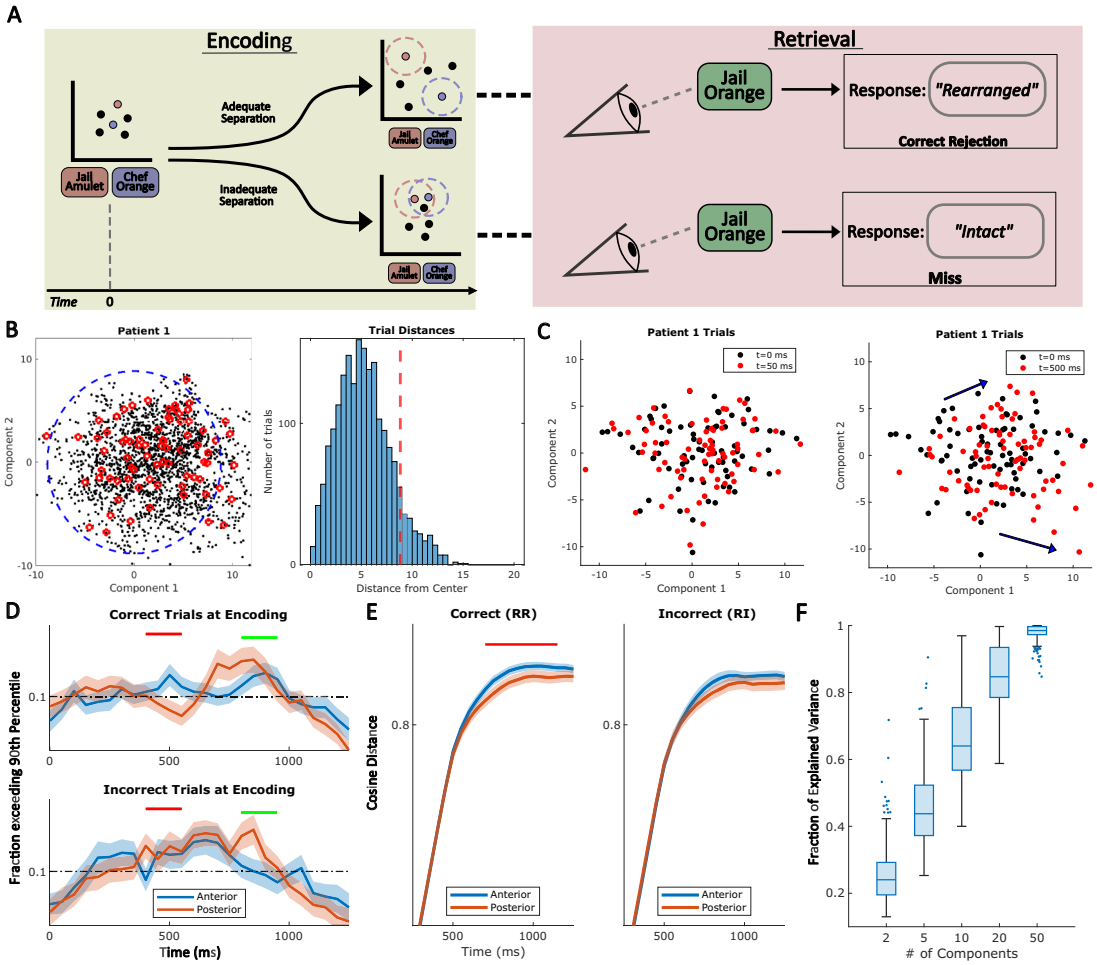

Fig. 5 | Subspace representational analysis of pattern separation. A Concept diagram depicting pattern separation at the time of study (item encoding). The colored dots under 'encoding' represent feature vectors that were either adequately separated or inadequately separated over time, while the black dots represent other word-pairs presented for an example patient. Under retrieval, the behavioral performance of the patient is shown for both adequately and inadequately separated items. The black dots in (**B**) depict feature vectors of all epochs of 1 patient. The blue dashed line represents the 90th percentile distance of all vectors, and the red circles represent all features during a given epoch. **C** shows the evolution of feature vectors, with angular divergence leading to increased cosine distance along the time series. **D** Fraction of Euclidean distances that exceed the 90th percentile over the entire time-series for correct (R-R) and incorrect (R-I) encoding trials using the first 20 principal components. A linear mixed-effects model was used to predict distance fraction using 'Region' and 'Condition', with subjects as the random effects. The data are represented as mean fraction +/- SEM. The green bar represents consistent regional effects, while red shows the interaction between region and condition (with FDR correction). **E** Average cosine distance between initial epoch and subsequent epochs across trials. Data are represented as mean fraction +/- SEM. Trials were under-sampled (10 trials randomly selected for each condition for each patient, and cosine distance was averaged over 500 iterations). Cosine distance ranges from 0 (angle in the same direction) to 1 (orthogonal) to 2 (opposite direction). Longitudinal difference was found through a t-test with multiple comparisons (with FDR correction). **F** Fraction of explained variance using the first 2, 5, 10, 20, and 50 principal components ($N = 328$ trials per box). Box plots show the median (center line), interquartile range (box), and the whiskers represent the range within 1.5× IQR from the lower and upper quartiles. Points beyond this are plotted as outliers.

provided evidence of greater functional differentiation (AH pattern separation signal that predicts recall).

Ripple Analysis

To test the interaction of theta oscillatory power with other neurophysiological properties, we examined ripple events, detected using parameters determined from recent consensus recommendations for human hippocampal ripples[58,59]. Figure 6 plots the ripple rate during the behavioral contrasts, which did not exhibit significant differences in our data. Correctly-recalled intact (I-I) items had a mean rate of 0.227 Hz (S.E. = 4.42e-3) in AH and 0.237 Hz (S.E. = 5.48e-3) in PH; associative misses (I-R) items had a mean rate of 0.218 Hz (S.E. = 6.30e-3) in AH and 0.235 Hz (S.E. = 7.25e-3) in PH; correctly reject new items (N-N) items had a mean rate of 0.233 Hz (S.E. = 5.91e-3) in AH and 0.235 (S.E. = 6.35e-3) in PH; and complete misses (X-N) items had a mean rate of 0.244 Hz (S.E. = 5.57e-3) in AH and 0.227 Hz (S.E. = 6.24e-3) in PH. To ensure robustness, we conducted the analysis again, varying the parameters to assess their impact on the results (Supplemental Fig. 4), which again did not exhibit significant differences in rate. Data of a complementary detection method (Supplemental Fig. 4C) show converging results. Analysis of ripple phase locking revealed significant non−uniformity for intact items across the theta frequency range in both AH and PH. For slow theta, I-I items exhibited significant non−uniformity along the entire hippocampus (mean phase for I-I anterior: $\theta = 119°$, R = 0.0692, $p = 0.0242$; I-I posterior: $\theta = -8°$, R = 0.0842, p = 0.0038; N-N anterior: $\theta = 42°$, R = 0.0316, $p = 0.5008$; N-N posterior $\theta = 31°$, R = 0.052, $p = 0.0955$). For the I-I events, we tested the difference in median phase angle between AH and PH, which revealed a significant offset of 127° after balancing for sample sizes (sampling 100 phases for 50,000 iterations; Watson-Williams test: F(1, 198) = 25.09, $p = 2.365e-6$). We concluded that slow theta power changes that occur during processing of intact items is

https://doi.org/10.1038/s41467-025-61464-z

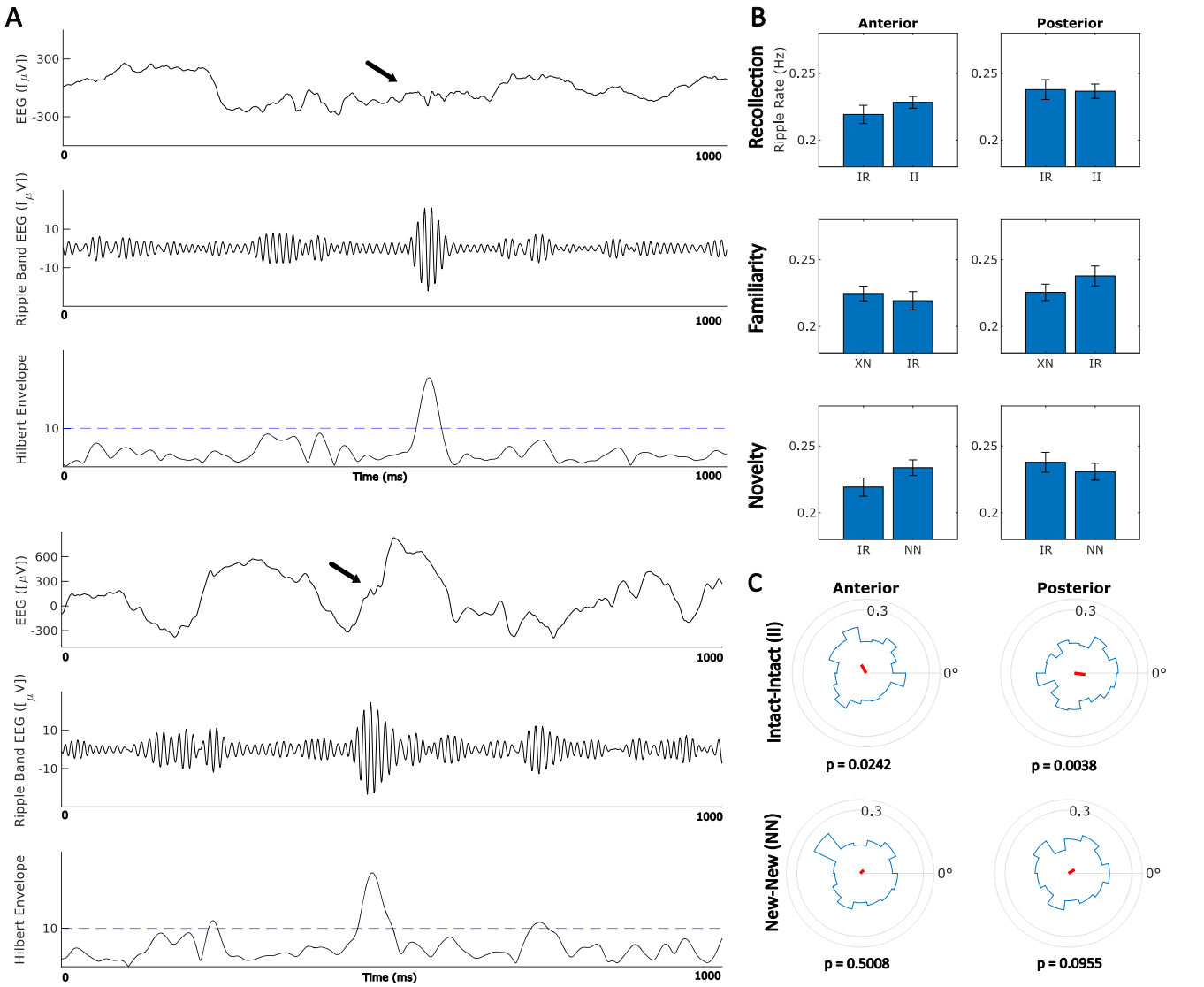

Fig. 6 | Longitudinal differences in hippocampal ripples. A Example of two identified ripples from two separate electrodes of a given patient using the Vaz 2019 detection method. On each plot, the arrow points to a ripple detected on raw EEG (though with removed line noise). The ripple band plot shows the bandpassed EEG 80–120 Hz, and Hilbert amplitude is shown for this band in the subsequent plot. **B** Ripple rates ($N = 360$ electrodes) for each defined contrast, counted from stimulus onset (0 ms) to the end of the time series (1800 ms). Data are represented as mean fraction ±SEM. Significance testing was done for each contrast at each region, which did not reveal any statistically significant differences for rate (Two-sample T-test, $p = 0.2571$, 0.5346, and 0.1069 for Anterior Recollection, Familiarity, and Novelty effects respectively, and p=0.8967, 0.2019, and 0.4694 for Posterior Recollection, Familiarity, and Novelty effects, respectively). No corrections for multiple comparisons were made as none of the results were significant. **C** Theta phase-locking of ripples starting at 1000 ms, correlating to visible power changes seen in the power modulation analysis, with sample sizes balanced and theta-axis scaled using PDF normalization ($N = 5990$ phase samples for Anterior II, $N = 4719$ for Posterior II, $N = 2584$ for Anterior NN, and $N = 1940$ for Posterior NN). In slow theta, Intact-Intact items displayed phase non-uniformity in both AH and PH after balancing sample sizes (Rayleigh's Z-test for non-uniformity; an undersampling technique was used by selecting and testing 1000 random phases for 500 iterations) and correcting for multiple comparisons (FDR Q = 0.05). No effects were observed for New-New items at this epoch.

associated with phase locking of ripple events. The phase differences of ripple–related phase locking may imply slight differential timing in anterior versus posterior processing of these events, and quantification of ripples raises the possibility of using co-rippling activity in salience versus posterior medial networks to understand differential participation for recollected versus novel items[60].

CA3 vs. CA1

As described in the Introduction, human hippocampal anatomy is characterized by notable differences in the relative proportion occupied by CA3/DG vs CA1 across the longitudinal axis (see[4] for 3D reconstruction of subfields from MRI). Therefore, we wanted to test whether the longitudinal differences in theta power were predicated upon precise intra-hippocampal recording location (as an alternative explanation for longitudinal differences). To address this issue, we reviewed the precise electrode location across hippocampal subfields for 23 subjects. For this analysis, electrodes were restricted to the AH, where the anatomical sub–localization was more reliable (i.e., electrodes could be confidently assigned to one subregion without crossing boundaries between them, visualized in Fig. 7A–C). The resulting plots, shown in Fig. 7E, suggest that the slow theta power increases observed during recollection may be driven principally by CA1 activity versus CA3 for novel items. The erratic nature of fast theta, again, makes it challenging to derive meaningful behavioral interpretations. These conclusions are somewhat limited by the difficulty in executing this analysis for posterior hippocampal

https://doi.org/10.1038/s41467-025-61464-z

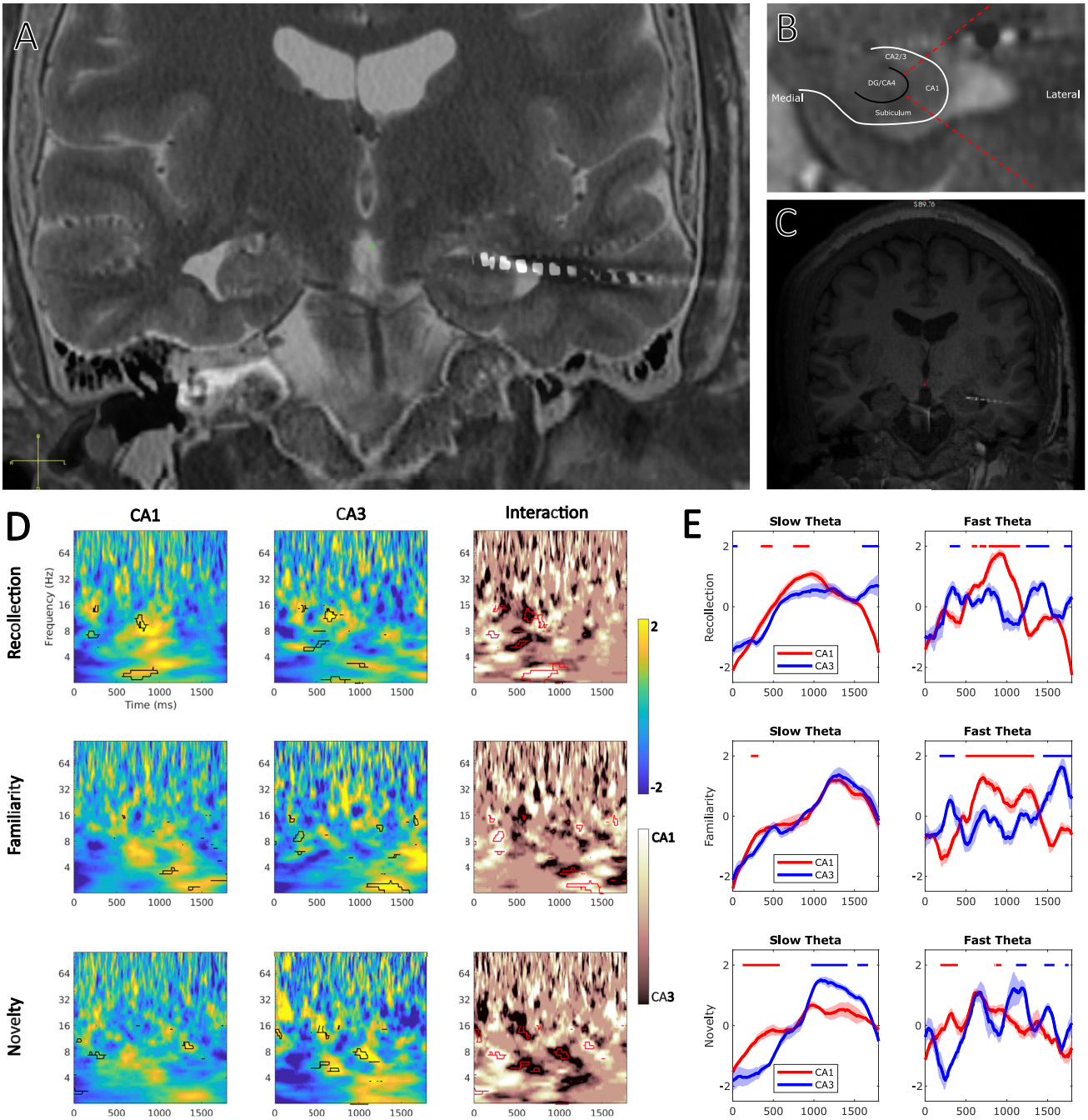

Fig. 7 | Analysis of electrodes localized to CA1. A Anterior slice from a T2-coronal MRI of a patient portraying a left-sided depth electrode with the first contact (most distal) in CA3. **B** Example diagram of sub-regional segmentation within a different slice of the same patient from *A*, based on a previously defined protocol. **C** T1 sequence of *A* with less visible artifacts for visualization. **D** Time-frequency plots of normalized power for CA1, CA3, and interaction between 'Region' (CA1 vs CA3) and 'Condition' which are contrasts corresponding for each memory effect (recollection, familiarity, novelty) similar to previous power analyses. Areas circled in black are time-frequency points during which contrast for each memory effect (I-I > I-R for recollection, I-R > X-N, and N-N > I-R) are significant. FDR was used for multiple comparisons correction. **E** Normalized power aggregate for slow and fast theta, with data being represented as mean +/- SEM.

electrodes, although the relatively modest theta power differences across the subfield recordings imply that subfield differences alone do not account for the longitudinal differentiation observed in our initial tests.

Discussion

Our results provide in-human electrophysiological data demonstrating anterior/posterior hippocampal differences in the processing of novel, familiar, and recollected items, as well as brain recordings to describe the temporal dynamics of pattern separation and pattern completion processes across the hippocampal longitudinal axis. Our findings establish mechanisms linking the AH with the processing of novel items, building on established connectivity relationships with regions implicated in salience[61]. Also, our data add a new dimension to conceptions of longitudinal specialization, as our analyses provide further evidence of longitudinal differences in recollection vs. familiarity–based item retrieval during associative memory using explicit behavioral contrasts established through previous characterization of human memory using the associative recognition paradigm.

Theories of hippocampal longitudinal specialization have evolved over the past three decades following initial publication by the Moser Lab describing the association between AH and affective contextual information[31]. Drawing on rodent data and early human non–invasive studies, the posterior hippocampus was linked with spatial processing. The next generation of theories incorporated the observation that the size of place cell fields in vary along the axis, with more precise spatial information represented in the posterior hippocampus[19,62]. The generalized application of this difference in the processing of specificity, termed 'gist/detail' models, posited that the human hippocampal exhibits analogous differences in the nature of information represented along the axis[18]. A version of this concept was proposed by Strange as well, linking more generalized representations in AH with semantic processing and cortical transfer[20]. Elevated theta band oscillatory power was observed in both AH and PH for recognition of novel items, although this was statistically greater (via two convergent statistical methods) in AH. We also noted that elevations in intra–hippocampal phase synchrony that characterize recollection were not present for the processing of novel items, in spite of grossly similar changes in power. This finding has some precedent in previous experiments that identify unique brain networks for novelty processing, linked with prefrontal circuitry supporting reward[63,64]. The null finding in our ripple analysis across memory contrasts is important to note, as a number of previous publications have suggested that ripple coupling is linked to behavioral performance in verbal and visual memory tasks[65,66]. Ripples have also been shown to have differing propagation pathways depending on the longitudinal location of CA1 in rodent data[67,68]. These results complement especially our connectivity analysis, which demonstrates enhanced intra-hippocampal synchronization for recollected items but not for the processing of novel items. The phase offset between anterior and posterior hippocampal ripples therefore provides further evidence of anterior/posterior hippocampal dissociation during the recovery of associative information, especially as compared to the processing of novel items. Further experimentation to describe these network differences (connectivity analyses) may further link processing of novel items in humans, and longitudinal differentiation, to such networks, building on differences in slow versus fast theta oscillatory differences that may uniquely support human memory[34,45].

We also report increased pre-stimulus phase synchrony for associative misses compared to correct intact items. The impact of pre-stimulus theta activity has been reported[69,70], and pre-stimulus functional connectivity has also been reported to mediate task performance[71]. We observed some evidence of these differences in our data, which may reflect temporal contiguity effects. Application of context models to associative memory data may provide a continuous estimate of behavioral states for interpreting these findings as part of the context maintenance and retrieval model (CMR2, see[72]) as applied to our AR paradigm.

Our results on their own certainly do not rule out alternative specialization asymmetries, including spatial or emotional. Rather, we provide direct electrophysiological evidence to support longitudinal asymmetries that include novelty processing and recollection, complementing fMRI experimentation[73] (although see Yebra et al. for countervailing information[74]). Salient items may elicit activation of ascending dopaminergic pathways mediated by salience networks, representing a potential mechanism for a 'boost' to encoding success observed for novel items[63,75]. An alternative novelty model involves rapid anterior/posterior hippocampal dissociation, occurring before our observed novelty effects, described by Lisman and Grace in their seminal work characterizing hippocampal–VTA circuits[76]. We note the plot shown in Supplemental Figure 2 maybe consistent with this model, which we view as complementary to our findings focused on theta oscillations, insofar as posterior hippocampal differences occur early in the time series (less than 200 msec after item onset). Our results suggest that a further set of experimentation that may flesh out conceptions of longitudinal specialization, including incorporation of emotional context information of varying complexity versus temporal or spatial complexity, which may alter the anterior/posterior activation balance we observe.

A logical question to ask of such representational models of longitudinal specialization is whether they pertain to concepts of familiarity versus recollection–based memory retrieval. Our results in this area were mixed, insofar as we observed longitudinal differences during recollection that may be consistent with gist/detail models, as presumably more representational information is recapitulated during recollection. However, the only differences we identified during familiarity–based recognition occurred late in the time series after item onset, which are harder to interpret. Further experimentation, using paradigms with different informational content, may help further elucidate this question.

Related to this point, previous conceptions of hippocampal longitudinal differentiation have not included explicit predictions regarding differences in pattern separation/completion. A hypothesized difference, however, is rooted in the anatomical distinctions between CA1-3 and DG distributions[3], as well as their respective roles in these processes. Ample evidence supports a pivotal role for DG in pattern separation[77–79], and CA3 neurons have evidence for a role in both pattern separation and completion ([47], reviewed in[46]). There is less support, however, for CA1 involvement in pattern separation, though its role in pattern completion remains a promising topic of investigation[47,80]. The relatively greater proportion of DG in the posterior hippocampus and CA1-3 in the anterior hippocampus may explain a longitudinal distinction in hippocampal function[18]. In support of this claim, fMRI data have shown longitudinal differences in activity during both pattern separation and completion tasks, with the former largely driven by CA3/DG activity, and the latter by CA1[78,81]. This hypothesized distinction has yet to be evaluated in humans using electrophysiology data, and it is therefore not obvious what predictions would follow for hippocampal longitudinal differences.

We introduce unique methods for quantifying pattern separation using the set of behavioral contrasts available within the associative recognition paradigm. Many experimental paradigms have been used to approximate pattern completion and separation, with commonalities that this association recognition paradigm can exploit. In pattern completion experiments, investigators have employed fragments of learned scenes[82], small changes to elements with complex events[83], and degraded or noisy cues[46], the choice of which may affect the pattern completion signal. In our task, a rearranged pair may be conceptualized as a noisy cue, and in order for a subject to successfully determine the 'rearranged' status, they must complete the pattern (original pair) based on this noisy cue. Memory tasks investigating pattern separation generally utilize a protocol that presents subjects with specific stimuli, and later requires them to identify stimuli that they previously encountered, are totally novel, or are similar but not the same as a prior stimulus. For example, the Mnemonic Similarity Task[50], a commonly used assay for pattern separation, uses this paradigm with targets, foils and lures, respectively. By analogy, the associative recognition paradigm presents a similar challenge by asking subjects to determine if a presented item pair is identical to a prior presentation (target), totally novel (foil), or rearranged (i.e., similar but inexact, i.e., lure). Our metric demonstrate functional effects, with significantly greater differentiation for successful rejections. The method is temporally precise, which thereby permits characterization of the temporal dynamics of pattern separation and completion, moving beyond analyses available via non–invasive methods. This revealed both anterior and posterior hippocampal activity during both pattern separation and completion, but with distinct temporal dynamics. Extension of these methods to incorporate formal behavioral modeling may permit imputation of pattern separation and completion signals.

Pattern completion activity has previously been attributed to the CA3 subregion, due to its ability within the hippocampus to maintain highly similar output despite varying input signals from the EC via the perforant pathway, or DG through mossy fibers[84]. This pattern-completing behavior, in part, is theorized to be due to self-projection by the CA3 pyramidal cells through recurrent collaterals, forming the anatomic basis for the auto-association networks studied through fMRI and rodent local-field potential EEG records[47]. In a more abstract sense, these networks also may result in attractor dynamics within the hippocampus, which is defined as stable states within a system that attract nearby, less stable states towards them[85]. Both attractor dynamics as well as the pattern-separated inputs from DG are the reasons why CA3 is thought to exhibit the so-called 'sigmoidal relationship' between input and output signal, as it is able to exhibit both separation and completion behaviors[46]. The relatively commensurate pattern separation/pattern completion activity that we observed may in turn explain why our data did not suggest substantial differences when limiting our analysis to CA1 versus CA3 localized electrodes, although anatomical issues limited this analysis to the AH.

We note that our pattern completion analysis assumed a 'recall to reject' framework for the processing of rearranged pairs, by which a subject first retrieves distinct memory traces linked with each item and then determines that the association has been rearranged (novel associative information), leading to successful rejection[86]. This model facilitated the pattern completion analysis described above. However, we acknowledge that alternative frameworks include simultaneous familiarity–based recognition for the retrieval of these word pairs, or match-mismatch detection of an associative pattern. This model assumes a dual–process framework. The former would include possibilities for the 'unitization' of encoded pairs, or the formation of a single item out of any arbitrary pair, which would allow familiarity to support correct rejection[87–89].

Match-mismatch detection, another possible model for interpretation of signal during processing of rearranged pairs at test, supposes the prediction of an upcoming or paired item to generate a detectable mismatch signal, and has been shown in non–invasive studies[90,91]. In such data, questions arise as to the precise nature of this signal, as it's unclear whether the signal of interest comes from the processing of associative novelty, or some other effect akin to recollection (an A-B-C-D sequence during encoding would trigger mismatch signals for A-B-D-C retrieval sequence, but would not for completely rearranged sequence like C-A-D-B or when there is no corresponding encoding signal during retrieval)[92]. Comparing rearranged items at encoding and retrieval would therefore be compatible with this model as a whole, as a detectable signal could be broadly labeled as 'mismatch,' but the further categorization would require a 3-way comparison with novel items during retrieval.

In summary, by analyzing oscillation-related behavioral effects and memory processes in epilepsy patients, we uncovered evidence of hippocampal longitudinal specialization, especially during the processing of novel memory items. The anterior hippocampus exhibits unique increases in theta band oscillatory power from 1000–1500 msec after item onset which was not characterized by enhanced anterior/posterior connectivity (unlike recollection). Finally, we demonstrated that locations along the hippocampal axis interact to affect pattern separation and pattern completion during item encoding and retrieval using a novel subspace representational approach. Our findings support the development of updated functional and computational models of hippocampal longitudinal specialization that incorporate these insights.

Methods

This study complies with ethical regulations for human research and was approved by the Institutional Review Board (IRB) at UT Southwestern Medical Center (UTSW). Patient's self-reported sex is described in Table 1 and was not considered under the study design, as only those with medical indications for electrode implantation were included.

Under stereotactic guidance, EEG electrodes were placed in 32 treatment-resistant epilepsy patients to aid seizure localization. These patients were under care at UTSW epilepsy monitoring unit where they consented to this study. Electrode placements were determined by the patient's clinical needs, and locations were then confirmed with the aid of a neuroradiologist. There were 19 additional patients excluded due to inadequate trials (< 8 for each condition) or not meeting our a priori behavioral performance metrics (pIntact | Intact − pIntact | Rearranged; discussed below). The table includes 32 patients (mean age = 36, std. dev. = 11, min. electrodes = 1, max. electrodes = 28, 15 female, 17 male, 26 right-handed (Table 1)). Electrodes counted for initial screening were those from AH, PH, EC, parahippocampus (PHC), PCC, and amygdala. We acknowledge the concern of intractable epilepsy distorting EEG signal and affecting quality; however, we opted to include electrodes within the same hemisphere of seizure onset, as physiological patterns characteristic of successful mnemonic processing have been included in analyses, especially for rare (simultaneously acquired) recordings from the anterior and posterior hippocampus[93]. Human non–invasive studies have also noted functional differences between AH and PH, which is independent of potential intractable epilepsy effects from sEEG recordings[94].

Behavioral Task

Subjects performed an associative recall task, which comprised of the encoding-distractor-retrieval paradigm broken down into multiple sections. The task was completed on a laptop at the patient's bedside, with the experimental task written in PyEPL, a programming library for experimental design[95]. Patients studied a pair of semantically unrelated nouns that follow word association norms[96] that were presented sequentially. 240 word pairs were presented in the encoding phase. 160 of those initial 240 would be presented during retrieval unmodified, while 80 would be shuffled for the 'rearranged' condition. An additional 80 words never before seen by the patient would be introduced during retrieval, which comprises the 'novel' condition. This totals up to 320 word pairs during retrieval (Fig. 8).

Patients were given the task instructions ahead of time, with the completion of a practice session before performing the experiment. Participants performed a version of the classical associative recognition episodic memory paradigm, illustrated in Fig. 8C. This version has been extensively implemented in adults across the lifespan in non-invasive experiments[28,97,98]. During the study phase of the associative memory task, patients were instructed to remember the pair of items shown on the screen. To encourage elaborative encoding and improve performance, participants were instructed to select which item would fit or go into the other (i.e., for SYRINGE and SUITCASE, participants selected SYRINGE). The associative pair was shown in white for 2 s. It then switched to blue, at which time the participant responded according to the catch criteria (which item fits within the other). This process is repeated for all 120 word pairs. The study phase is followed by a math distractor task, during which the patients add 3 single-digit numbers (A + B + C) for 30 s. The participants then take a timed 5-min break before continuing onto the test task. For this phase, word pairs of the three previously described categories (intact, rearranged, novel) are presented in random order. Similarly, participants have 2 s while the words appeared white on the screen to prepare before responding 'same' to intact pairs, 'rearranged' to rearranged pairs, and 'new' to novel pairs via button press. From these responses, word pairs were categorized as a combination of their true status vs. the patient's actual response. For example, 'intact-intact' would denote an associative hit in which the patient correctly identified a pair they have seen before, while 'intact-rearranged' would denote an associative miss where the patient responded 'rearranged' despite being presented the same

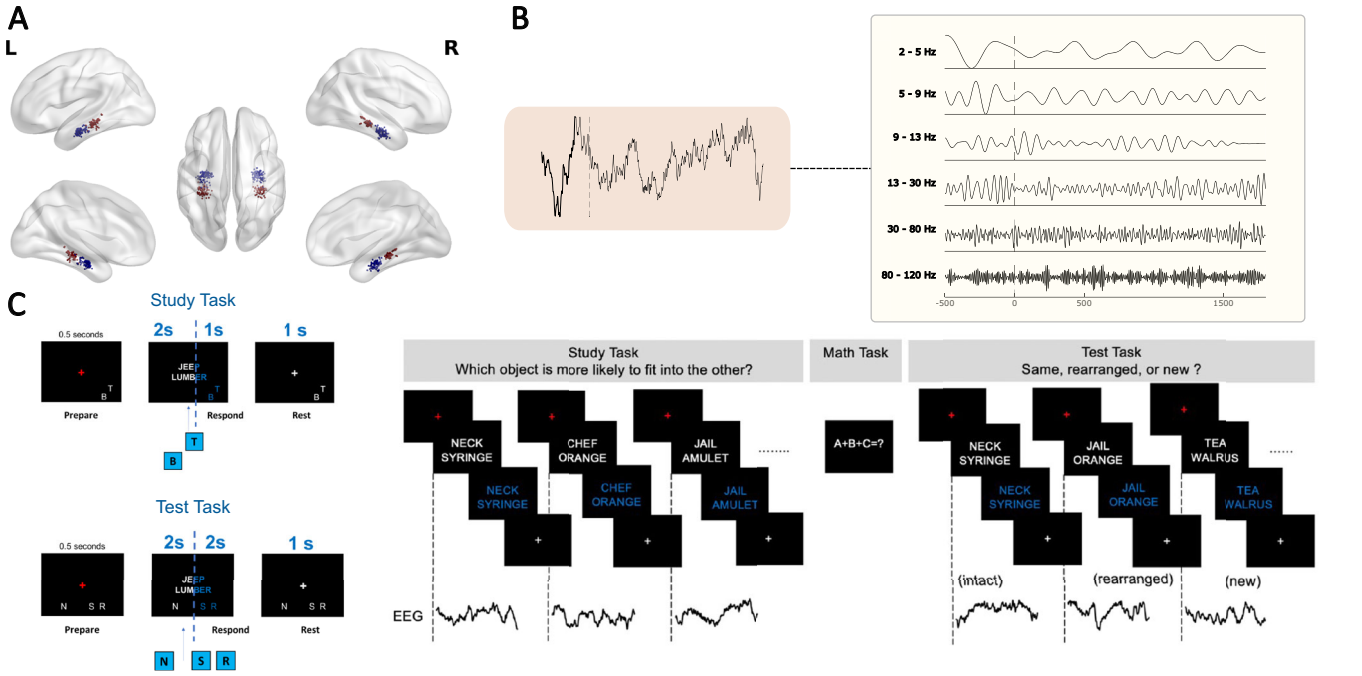

Fig. 8 | Description of the associative recognition paradigm. A Electrode distribution for anterior and posterior hippocampus. **B** Local field potential (LFP) signal decomposition. **C** Left diagram shows structure of trials during encoding (study) and retrieval (test). The 'B' response denotes whether the bottom word within an encoding pair goes into the top word, while vice versa for the 'T' response. The right diagram depicts experimental paradigm for 1 patient session.

word pair previously during the study phase. Rearranged pairs require participants to correctly recall the associate of both items to accurately classify the item as 'rearranged-rearranged'.

Response timing is measured from the start of word appearance on the screen (white), but before the participant response period. Word pairs during both the study and test phases were preceded with a red cross centered on the screen for 0.5 s, and followed by 1 s with a 200 ms jitter of a white cross after the word pair disappears from screen.

Behavioral results were accounted for in selecting patient for iEEG analysis, and thus probability of recollection (*pR*) was used. This metric is defined by the difference between the proportion of correctly–identified intact pairs and the proportion of rearranged pairs that were incorrectly labeled as intact, similar to previous studies[97]. Rationale for implementing this metric includes selecting for patients who are appropriately engaged in the task and engaging neural resources that would allow them to perform above chance as well as connecting our findings to previous reports that used non–invasive imaging[28].

Signal Processing

EEG Pre-processing. A total of 32 patients with electrodes in our regions of interest, which included AH, PH, EC, and parahippocampus were included in this study. These regions were confirmed by an independent neuroradiologist, and the uncal notch was used as an anatomical landmark to delineate AH from PH. These patients had a varying number of electrodes across regions (see Fig. 1C). EEG signals were recorded in Nihon Kohden 2100 Clinical Systems and processed using MATLAB (2023a). These signals were sampled at 1000 Hz and used the average referencing paradigm, which measured individual electrode signals as the voltage difference between each electrode and the average of all implanted electrodes. Channels with significant interictal activity, were identified by an epileptologist and removed from the analysis. Epochs for analysis were identified as the 1800 ms immediately following the appearance of words on screen during both the encoding (study) and retrieval (test) phases of the experiment. A Butterworth filter with a bandwidth of 4 Hz to centered at 60 Hz up to its 2nd harmonic was applied to the iEEG signal at the trial level. Noisy channels were identified by measuring kurtosis, which is a measure for 'tailedness' of a distribution (ratio of fourth central moment to the fourth power of standard deviation). Distributions with a kurtosis greater than 4 were deemed to contain too many artifacts and thus removed[28,33]. We also implemented a median-based filtering technique to further remove remaining artifacts[99] (summarized in Fig. 1D). Briefly, this technique labels trials with signals greater than the 95th percentile as 'artifacts' and removes them from the analysis.

Power Spectrum Analysis. For each epoch, we used a Morlet-wavelet transformation (with width of 6) to obtain trial-level power at each time point and frequency band, which are log-spaced from 2 to 120 Hz resulting in 48 frequency steps. To account for inter-electrode power variations, power per trial at each frequency band was then normalized to the individual electrode's baseline, which is denoted as the 1000 milliseconds preceding the word pair stimulus.

$$P_n(f,e) = \frac{P(f) - \mu_{baseline}(f)}{\sigma_{baseline}(f)} \quad (1)$$

where f are the frequency bands and e are individual electrodes. In order to determine whether differences exist between regions and behavioral task outcomes, we generated time–frequency plots of oscillatory power for conditions based on participants responses at test, such as intact/intact items, which are those which were correctly identified as being matched with appropriate associate when queried (associative hits). Conditions we took into account were I-I (intact-intact), N-N (new-new), associative misses (I-R and R-I), as well as complete misses, which we defined as 'intact' or 'rearranged' pairs that were incorrectly labeled as 'novel' during retrieval. Our three main contrasts of interest are recollection (I-I > I-R), familiarity (I-R > [R-N and I-N], or in other words, I-R > X-N, to compare associative misses

against complete misses), and novelty (N-N > I-R). To mitigate unbalanced sample sizes, only electrode pairs with at least 8 word-pairs in every condition were kept. The power data was then more robustly analyzed through a linear mixed-effects model (LMEM), which was used due to its ability to analyze the 'fixed effects' of interest in the context of 'random effects' introduced by group variability. Our power model in Wilkinson's notation was:

$$\begin{aligned}\text{NormPow} \sim 1 + \text{Condition} + \text{Condition:Region} + \text{Region} \\ + 1|(\text{Subject/Electrode})\end{aligned} \quad (2)$$

with the random term consisting of effects by subject as well as electrodes within each subject. We used EC as our reference region in the model. The outputs of these models were adjusted for the type I error introduced in multiple comparisons by using the false discovery rate (FDR for $p < 0.05$, $Q = 0.05$) algorithm. Post hoc comparisons were defined for each statistical question using the estimates from the LMEM, and tested using MATLAB's built-in function for coefficient testing. Degrees of freedom estimation were generated using Satterthwaite's correction. Significant effects denoted on time-frequency plots were oscillatory power of a given condition (rearranged-rearranged, novel-novel, etc.) that was greater than incorrect pairs (associative misses), which included intact-rearranged and rearranged-intact conditions. Additionally, the individual interaction terms for each condition-region combinations were aggregated to determine the overall interaction effect between 'condition' and 'region.' As a complementary method to confirm our LMEM results, we subsequently ran an ANOVA model, consisting of randomly assigned labels for 500 iterations following similar work[100], using the same contrasts of interest to compare with the mixed-effects model.

Phase Synchrony along the Hippocampus. In order to further characterize our power results, with significant interactions depicted in both slow and fast theta, we next analyzed phase synchrony of electrodes between AH and PH within these two bands (2–5 Hz for slow theta and 5–9 Hz for fast theta), which are defined similarly in previous work[28]. Synchrony is broadly defined as the phase difference between two given oscillators[101]:

$$\phi_{n,m} = n\varphi_1 - m\varphi_2 \quad (3)$$

For signals in similar frequency bands, n and m can be canceled, leaving behind only the phase difference.

In this analysis, we utilized a bipolar re–referencing scheme which involves using an immediately adjacent contact on the same depth electrode to calculate voltage signal. A Butterworth bandpass filter was used to select for slow and fast theta, and the instantaneous phase for the specified frequency bands was obtained by calculating the angle of the complex signal produced by the Hilbert transform for the entire time series. Phase synchrony was measured for all possible combinations of electrode pairs within each hemisphere between the AH and PH. Phase synchrony was measured for all possible combinations of electrode pairs within each hemisphere between the AH and PH. For example, in a patient with 2 anterior and 3 posterior contacts in the left hippocampus, phase difference would be tested and measured across 2 AH–PH bipolar combinations. AH and PH are then thought to exhibit phase synchrony if the phase combinations tested are significantly non-uniform for at least half a cycle of theta. A Rayleigh's Z-test was then used on these phase differences to measure the degree of non–uniformity[102], with a significant Rayleigh's Z, stable for at least half a cycle, denoting synchrony. To balance for unequal sample sizes, an under-sampling technique was used where 10 trials were selected at random without replacement per electrode pair and the z-statistics obtained were aggregated over 1000 iterations[103]. Electrode pairs with under 10 word-pair trials were thrown out. To determine significant difference in non-uniformity during the time series, we ran a LMEM for each contrast (with subjects as the random effects), and used FDR (for $p < 0.05$, $Q = 0.05$) for correction for multiple comparisons. We repeated this analysis for slow and fast theta. Significant differences within each contrast that were shorter than half a cycle of the respective theta bands were removed. We additionally determined correlation between change in phase synchrony and power in order to confirm that power was not reliably predicting phase synchrony for all conditions within a region (Supplemental Fig. 3).

Temporal Dynamics Hippocampal Pattern Completion. We devised and implemented a procedure to quantify pattern completion through reinstatement during retrieval. This process involved measuring the divergence between cluster centroids in low-dimensional space for test pairs in which both items were presented during encoding but paired with different associates (rearranged pairs correctly identified as rearranged). This allowed us to measure the expected divergence in features between encoding and retrieval. The procedure involves selecting trials of the correctly–labeled rearranged word pairs during retrieval, as well as the two pairs during encoding that comprised the rearranged pair. Feature vectors, which are a multidimensional representation of oscillatory power at a given epoch, were obtained for each trial[104]. These vectors at encoding and retrieval are defined as:

$$\begin{aligned}\overrightarrow{\mathbf{E_{1,i}}} &= \{z_{1,1}(i), z_{1,2}(i), \ldots z_{l,f}(i), \ldots, z_{L,F}(i)\} \\ \overrightarrow{\mathbf{E_{2,i}}} &= \{z_{1,1}(i), z_{1,2}(i), \ldots z_{l,f}(i), \ldots, z_{L,F}(i)\} \\ \overrightarrow{\mathbf{R_i}} &= \{z_{1,1}(i), z_{1,2}(i), \ldots z_{l,f}(i), \ldots, z_{L,F}(i)\}\end{aligned} \quad (4)$$

where z represents normalized power averaged over a given epoch, $l = 1, 2, \ldots, L$ represents the number of electrodes belonging to a particular region, and f being the log-spaced frequency bands from 2 Hz to 120 Hz. Each temporal epoch i is defined as a 500-ms window with a 50-ms (90% overlap) with the previous epoch $i - 1$.

After generating the feature vectors, we performed a dimensionality reduction using principal component analysis (PCA) to project our data to a 2-dimensional space for every patient and hemisphere, shown in Fig. 4A–E. To obtain a measure of divergence between the encoding and retrieval feature vectors through time, we trained data using a k-means clustering algorithm with $k = 2$ and the center initialization parameter being the mean locations of the two groups. This was to mitigate potential faulty clustering where the local minima obtained from the cost function, which is determined using squared euclidean distance, converges with highly unbalanced clusters, such as a cluster with a single outlier point. We obtained the average centroid distances by aggregating all the electrodes for each hemispheric region (left AH, left PH, etc.) at each retrieval trial and the two associated encoding trials. We then combined data for each hemisphere after normalizing to the PCA coordinates. Distances were normalized with respect to the initial distances for each region; z-statistics were obtained for the difference between each region to 0, as well as between AH and PH. We used a cluster-based multiple comparisons correction ($p < 0.05$ for at least 50 ms consecutively) for both of these comparisons.

Our pattern completion methods are predicated on the 'recall-to-reject' framework (see Discussion), where successful recognition of rearranged items depends on recovering individual pairs at encoding. The selection of rearranged trials in this analysis allowed us to create conditions of similarity in stimulus analogous to MST paradigms typically used to investigate pattern completion and separation[50,52]. Because the number of components is unique for each patient due to the varying number of electrode contacts, the goal of this procedure was to quantify the difference between rearranged items in low-dimensional space to allow cross-patient comparisons. Evidence of information specific to each item within a pair should emerge over

time within this 'recall-to-reject' framework, and these features should exhibit similarity to those at encoding that emerges across time. The centroid analysis identifies when the similarity vector for a pair diverges from the overall distribution, consistent with successful pattern completion as schematized in Fig. 4.

Evidence of Pattern Separation. We devised a method to measure pattern separation by defining two unique distance measures for trials between conditions to determine whether there exist quantifiable measures of encoding items diverging through time. Feature vectors of 'rearranged' items were generated similarly to the methods previously described. 'Rearranged' items were used here as they allow the contrast between items where pattern separation succeeded versus items where pattern separation failed (see 5A). Pattern separation is an encoding-driven process for cued memory paradigms such as what we employed (see Discussion), and successful recollection is dependent on the adequate separation of associative features across trials. By comparing rearranged trials that were correctly rejected against rearranged trials that were incorrectly labeled as 'Intact,' during which pattern separation has failed, we can calculate a functional metric for the effects of pattern separation. The method we devised to generate a metric first uses PCA, which was applied to these vectors for all trials and epochs for each patient. Dimensionality reduction is crucial here as it 1) accounts for intersubject differences in feature dimensionality, such as electrode number, and 2) facilitates the Euclidean and cosine distance analysis. The Euclidean distance between the mean and each individual point was calculated for 20 main components, and subsequently, 2 and 50 components were calculated to verify the stability and asymptotic behavior of the distances, as dimensionality reduction has the potential to lose meaningful information. The fraction of trials whose distance from the mean exceeds the 90th percentile of the entire time series was generated per time point and aggregated across all patients. A mixed-effects model was run predicting the distance proportion through time using 'region' and 'condition,' the fixed effects ('subjects' were the random effects) for both correctly-identified rearranged trials and incorrect trials during encoding. Multiple comparison corrections (FDR for $p < 0.05$, $Q = 0.05$) was used.

We next evaluated the activity of individual trials through time by evaluating the cosine distance of correct and incorrect trials for each region. Feature vectors using power were obtained for the first 20 components, which were generated similarly to the previous method. For each trial, the cosine distance between the current epoch and the initial epoch was obtained and aggregated across all patients. To balance for unequal sample sizes, we used an under-sampling balancing technique to select for trials between conditions and averaged distances across 500 iterations[103]. We then tested the longitudinal difference for both correct and incorrect pairs, and corrected for multiple comparisons (FDR for $p < 0.05$, $Q = 0.1$).

Ripple Rate and Theta Phase-Locking. We next determined ripple rate across all word-pair conditions to evaluate for significant variability between these conditions. Ripple rate detection, based on previous work[65], involves a bandpass filter across the ripple band (80-120 Hz), followed by a Hilbert transform over the entire band to obtain amplitude as a function of time. We identified time periods in each trial where the Hilbert envelope, or the analytic signal's magnitude, was between 2 and 3 standard deviations above the mean. Periods of at least 20 ms were retained as ripples, and any ripples that were within 10 ms of each other were merged. There was no upper limit for ripple duration. Trials with kurtosis of over 4 were removed, as well as the median-based filtering for artifact removal that was previously described. Events were aggregated for each condition across all subjects and the rate from the time series was obtained. We then repeated this ripple detection method with different varying parameters for threshold detection (Hilbert envelope between 2 and 5 standard deviations), as well as different minimum duration (10 ms) (see[58] for summary of previously reported detection methods). A complementary ripple detection method using root-mean-square (RMS) of raw voltage was also used to confirm our findings (see[105]).

After obtaining the ripple rate across the longitudinal hippocampus, we analyzed slow theta phase in the AH and PH during the previously identified ripples at 1000 ms, which largely correlates with elevation in power from the previous power results. These phases were tested for non-uniformity to identify potential theta phase-locking that were consistent across trials and patients. Unequal sample sizes were balanced using an under-sampling technique that averaged non-uniformity scores over 500 iterations similar to previous analyses.

Hippocampal Sub-field Analyses. We next repeated select analyses with a smaller data set that directly compared CA1 and CA3 electrodes. There were 69 AH electrodes selected in 28 patients that could be determined to be CA1 or CA3 with the aid of the corresponding patient MRI. All electrodes were assigned to these subregions using high-resolution coronal T1 and T2 MR scans co-registered to post implantation imaging via independent review by clinicians with advanced neuro-anatomical training and expertise in localization of electrode contacts (example shown in 7A; see[4] for a detailed, illustrated protocol in subfield segmentation). We followed the same procedure for the power spectra analyses, by first obtaining power of the entire time-frequency spectrum for each word-pair condition, followed by processing using the same LMEM, only with 'CA1' and 'CA3' replacing 'AH' and 'PH' in our original model.

Reporting summary

Further information on research design is available in the Nature Portfolio Reporting Summary linked to this article.

Data availability

The processed EEG data generated in this study have been deposited in the Texas Data Repository (https://doi.org/10.18738/T8/GIZHOK)[106]. Raw clinical data are protected and are not available due to data privacy laws. Deidentified electrode data has been included in the Supplementary Information. Source data are provided with this paper.

Code availability

Code is available as a zip (Supplemental Code); additional code availability can be found by contacting Dr. Bradley Lega at bradley.lega@utsouthwestern.edu.

References

1. Ranganath, C. Binding items and contexts: The cognitive neuroscience of episodic memory. *Curr. Directions Psychological Sci.* **19**, 131–137 (2010).
2. Yim, H., Dennis, S. J. & Sloutsky, V. M. The development of episodic memory: Items, contexts, and relations. *Psychological Sci.* **24**, 2163–2172 (2013).
3. Malykhin, N. V., Lebel, R. M., Coupland, N. J., Wilman, A. H. & Carter, R. In vivo quantification of hippocampal subfields using 4.7 t fast spin echo imaging. *Neuroimage* **49**, 1224–1230 (2010).
4. Dalton, M. A., Zeidman, P., Barry, D. N., Williams, E. & Maguire, E. A. Segmenting subregions of the human hippocampus on structural magnetic resonance image scans: An illustrated tutorial. *Brain Neurosci. Adv.* **1**, 2398212817701448 (2017).
5. Hunsaker, M. R. & Kesner, R. P. Dissociations across the dorsal–ventral axis of ca3 and ca1 for encoding and retrieval of contextual and auditory-cued fear. *Neurobiol. Learn. Mem.* **89**, 61–69 (2008).
6. Kahn, M. C., Hough, G. E., Ten Eyck, G. R. & Bingman, V. P. Internal connectivity of the homing pigeon (columba livia) hippocampal

formation: an anterograde and retrograde tracer study. *J. Comp. Neurol.* **459**, 127–141 (2003).
7. Gasbarri, A., Packard, M. G., Campana, E. & Pacitti, C. Anterograde and retrograde tracing of projections from the ventral tegmental area to the hippocampal formation in the rat. *Brain Res. Bull.* **33**, 445–452 (1994).
8. Duvernoy, H. M. et al. The human hippocampus: functional anatomy, vascularization and serial sections with MRI, 3rd Edition, Springer, (2005).
9. Kier, E. L., Staib, L. H., Davis, L. M. & Bronen, R. A. Mr imaging of the temporal stem: anatomic dissection tractography of the uncinate fasciculus, inferior occipitofrontal fasciculus, and meyer's loop of the optic radiation. *Am. J. Neuroradiol.* **25**, 677–691 (2004).
10. Catenoix, H., Magnin, M., Mauguiere, F. & Ryvlin, P. Evoked potential study of hippocampal efferent projections in the human brain. *Clin. Neurophysiol.* **122**, 2488–2497 (2011).
11. Dolorfo, C. L. & Amaral, D. G. Entorhinal cortex of the rat: organization of intrinsic connections. *J. Comp. Neurol.* **398**, 49–82 (1998).
12. Kahn, I., Andrews-Hanna, J. R., Vincent, J. L., Snyder, A. Z. & Buckner, R. L. Distinct cortical anatomy linked to subregions of the medial temporal lobe revealed by intrinsic functional connectivity. *J. Neurophysiol.* **100**, 129–139 (2008).
13. Libby, L. A., Ekstrom, A. D., Ragland, J. D. & Ranganath, C. Differential connectivity of perirhinal and parahippocampal cortices within human hippocampal subregions revealed by high-resolution functional imaging. *J. Neurosci.* **32**, 6550–6560 (2012).
14. Poppenk, J. & Moscovitch, M. A hippocampal marker of recollection memory ability among healthy young adults: contributions of posterior and anterior segments. *Neuron* **72**, 931–937 (2011).
15. Kim, H. Encoding and retrieval along the long axis of the hippocampus and their relationships with dorsal attention and default mode networks: The hernet model. *Hippocampus* **25**, 500–510 (2015).
16. Maguire, E. A. et al. Navigation-related structural change in the hippocampi of taxi drivers. *Proc. Natl. Acad. Sci. USA* **97**, 4398–4403 (2000).
17. Richardson, M. P., Strange, B. A. & Dolan, R. J. Encoding of emotional memories depends on amygdala and hippocampus and their interactions. *Nat. Neurosci.* **7**, 278–285 (2004).
18. Poppenk, J., Evensmoen, H. R., Moscovitch, M. & Nadel, L. Long-axis specialization of the human hippocampus. *Trends Cogn. Sci.* **17**, 230–240 (2013).
19. Kjelstrup, K. B. et al. Finite scale of spatial representation in the hippocampus. *Science* **321**, 140–143 (2008).
20. Strange, B. A. & Dolan, R. J. Anterior medial temporal lobe in human cognition: Memory for fear and the unexpected. *Cogn. neuropsychiatry* **11**, 198–218 (2006).
21. Kishiyama, M. M., Yonelinas, A. P. & Lazzara, M. The von restorff effect in amnesia: the contribution of the hippocampal system to novelty-related memory enhancements. *J. Cogn. Neurosci.* **16**, 15–23 (2004).
22. de Chastelaine, M., Mattson, J. T., Wang, T. H., Donley, B. E. & Rugg, M. D. Independent contributions of fmri familiarity and novelty effects to recognition memory and their stability across the adult lifespan. *NeuroImage* **156**, 340–351 (2017).
23. Tulving, E., Markowitsch, H. J., Craik, F. I., Habib, R. & Houle, S. Novelty and familiarity activations in pet studies of memory encoding and retrieval. *Cereb. Cortex* **6**, 71–79 (1996).
24. Kafkas, A. & Montaldi, D. How do memory systems detect and respond to novelty? *Neurosci. Lett.* **680**, 60–68 (2018).
25. Jacobs, J. et al. Direct recordings of grid-like neuronal activity in human spatial navigation. *Nat. Neurosci.* **16**, 1188–1190 (2013).
26. Jutras, M. J., Fries, P. & Buffalo, E. A. Oscillatory activity in the monkey hippocampus during visual exploration and memory formation. *Proc. Natl Acad. Sci. USA* **110**, 13144–13149 (2013).
27. Umbach, G. et al. Time cells in the human hippocampus and entorhinal cortex support episodic memory. *Proc. Natl. Acad. Sci. USA* **117**, 28463–28474 (2020).
28. Kota, S., Rugg, M. D. & Lega, B. C. Hippocampal theta oscillations support successful associative memory formation. *J. Neurosci.* **40**, 9507–9518 (2020).
29. Ayhan, F. et al. Resolving cellular and molecular diversity along the hippocampal anterior-to-posterior axis in humans. *Neuron* **109**, 2091–2105 (2021).
30. Costa, M. et al. Aversive memory formation in humans involves an amygdala-hippocampus phase code. *Nat. Commun.* **13**, 6403 (2022).
31. Moser, M.-B. & Moser, E. I. Functional differentiation in the hippocampus. *Hippocampus* **8**, 608–619 (1998).
32. Zhang, H., Watrous, A. J., Patel, A. & Jacobs, J. Theta and alpha oscillations are traveling waves in the human neocortex. *Neuron* **98**, 1269–1281 (2018).
33. Lin, J.-J. et al. Theta band power increases in the posterior hippocampus predict successful episodic memory encoding in humans. *Hippocampus* **27**, 1040–1053 (2017).
34. Gedankien, T. et al. Acetylcholine modulates the temporal dynamics of human theta oscillations during memory. *Nat. Commun.* **14**, 5283 (2023).
35. Staresina, B. P., Fell, J., Do Lam, A. T., Axmacher, N. & Henson, R. N. Memory signals are temporally dissociated in and across human hippocampus and perirhinal cortex. *Nat. Neurosci.* **15**, 1167–1173 (2012).
36. Mitchell, S. J. & Ranck Jr, J. B. Generation of theta rhythm in medial entorhinal cortex of freely moving rats. *Brain Res.* **189**, 49–66 (1980).
37. Alonso, A. & Garcia-Austt, E. Neuronal sources of theta rhythm in the entorhinal cortex of the rat: I. laminar distribution of theta field potentials. *Exp. brain Res.* **67**, 493–501 (1987).
38. Hasselmo, M. E. What is the function of hippocampal theta rhythm?–linking behavioral data to phasic properties of field potential and unit recording data. *Hippocampus* **15**, 936–949 (2005).
39. O'keefe, J. & Burgess, N. Dual phase and rate coding in hippocampal place cells: theoretical significance and relationship to entorhinal grid cells. *Hippocampus* **15**, 853–866 (2005).
40. Jensen, O. & Lisman, J. E. Hippocampal sequence-encoding driven by a cortical multi-item working memory buffer. *Trends Neurosci.* **28**, 67–72 (2005).
41. Seidenbecher, T., Laxmi, T. R., Stork, O. & Pape, H.-C. Amygdalar and hippocampal theta rhythm synchronization during fear memory retrieval. *Science* **301**, 846–850 (2003).
42. Huerta, P. T. & Lisman, J. E. Bidirectional synaptic plasticity induced by a single burst during cholinergic theta oscillation in ca1 in vitro. *Neuron* **15**, 1053–1063 (1995).
43. Wang, D. X., Schmitt, K., Seger, S., Davila, C. E. & Lega, B. C. Cross-regional phase amplitude coupling supports the encoding of episodic memories. *Hippocampus* **31**, 481–492 (2021).
44. Seger, S. E., Kriegel, J. L., Lega, B. C. & Ekstrom, A. D. Memory-related processing is the primary driver of human hippocampal theta oscillations. *Neuron* **111**, 3119–3130 (2023).
45. Choi, K. et al. Longitudinal differences in human hippocampal connectivity during episodic memory processing. *Cereb. cortex Commun.* **1**, tgaa010 (2020).
46. Yassa, M. A. & Stark, C. E. Pattern separation in the hippocampus. *Trends Neurosci.* **34**, 515–525 (2011).
47. Rolls, E. T. Pattern separation, completion, and categorisation in the hippocampus and neocortex. *Neurobiol. Learn. Mem.* **129**, 4–28 (2016).
48. Kyle, C. T., Stokes, J. D., Lieberman, J. S., Hassan, A. S. & Ekstrom, A. D. Successful retrieval of competing spatial environments in

humans involves hippocampal pattern separation mechanisms. *elife* **4**, e10499 (2015).
49. Robin, J. & Moscovitch, M. Details, gist and schema: hippocampal–neocortical interactions underlying recent and remote episodic and spatial memory. *Curr. Opin. Behav. Sci.* **17**, 114–123 (2017).
50. Stark, S. M., Kirwan, C. B. & Stark, C. E. Mnemonic similarity task: A tool for assessing hippocampal integrity. *Trends Cogn. Sci.* **23**, 938–951 (2019).
51. Srokova, S., Aktas, A. N., Koen, J. D. & Rugg, M. D. Dissociative effects of age on neural differentiation at the category and item levels. *J. Neurosci.* **44** (2024).
52. Leal, S. L. & Yassa, M. A. Integrating new findings and examining clinical applications of pattern separation. *Nat. Neurosci.* **21**, 163–173 (2018).
53. de Chastelaine, M., Mattson, J. T., Wang, T. H., Donley, B. E. & Rugg, M. D. The neural correlates of recollection and retrieval monitoring: Relationships with age and recollection performance. *Neuroimage* **138**, 164–175 (2016).
54. Thakral, P. P., Sarah, S. Y. & Rugg, M. D. The hippocampus is sensitive to the mismatch in novelty between items and their contexts. *Brain Res.* **1602**, 144–152 (2015).
55. Menon, V. & Uddin, L. Q. Saliency, switching, attention and control: a network model of insula function. *Brain Struct. Funct.* **214**, 655–667 (2010).
56. Staresina, B. P. et al. Hippocampal pattern completion is linked to gamma power increases and alpha power decreases during recollection. *elife* **5**, e17397 (2016).
57. Kolibius, L. D. et al. Hippocampal neurons code individual episodic memories in humans. *Nat. Hum. Behav.* **7**, 1968–1979 (2023).
58. Liu, A. A. et al. A consensus statement on detection of hippocampal sharp wave ripples and differentiation from other fast oscillations. *Nat. Commun.* **13**, 6000 (2022).
59. Kunz, L. et al. Ripple-locked coactivity of stimulus-specific neurons and human associative memory. *Nat. Neurosci*. 1–13 (2024).
60. Cowan, E. T., Fain, M., O'Shea, I., Ellman, L. M. & Murty, V. P. Vta and anterior hippocampus target dissociable neocortical networks for post-novelty enhancements. *J. Neurosci.* **41**, 8040–8050 (2021).
61. Zheng, J. et al. Amygdala-hippocampal dynamics during salient information processing. *Nat. Commun.* **8**, 14413 (2017).
62. Knierim, J. J. The hippocampus. *Curr. Biol.* **25**, R1116–R1121 (2015).
63. Bunzeck, N., Doeller, C. F., Dolan, R. J. & Duzel, E. Contextual interaction between novelty and reward processing within the mesolimbic system. *Hum. brain Mapp.* **33**, 1309–1324 (2012).
64. Camara, E., Rodriguez-Fornells, A. & Münte, T. F. Functional connectivity of reward processing in the brain. *Front. Hum. Neurosci.* **2**, 419 (2009).
65. Vaz, A. P., Inati, S. K., Brunel, N. & Zaghloul, K. A. Coupled ripple oscillations between the medial temporal lobe and neocortex retrieve human memory. *Science* **363**, 975–978 (2019).
66. Norman, Y. et al. Hippocampal sharp-wave ripples linked to visual episodic recollection in humans. *Science* **365**, eaax1030 (2019).
67. Patel, J., Schomburg, E. W., Berényi, A., Fujisawa, S. & Buzsáki, G. Local generation and propagation of ripples along the septotemporal axis of the hippocampus. *J. Neurosci.* **33**, 17029–17041 (2013).
68. Tingley, D. & Buzsáki, G. Routing of hippocampal ripples to subcortical structures via the lateral septum. *Neuron* **105**, 138–149 (2020).
69. Addante, R. J., Watrous, A. J., Yonelinas, A. P., Ekstrom, A. D. & Ranganath, C. Prestimulus theta activity predicts correct source memory retrieval. *Proc. Natl Acad. Sci.* **108**, 10702–10707 (2011).
70. Merkow, M. B., Burke, J. F., Stein, J. M. & Kahana, M. J. Prestimulus theta in the human hippocampus predicts subsequent recognition but not recall. *Hippocampus* **24**, 1562–1569 (2014).
71. Sherwin, J. S., Muraskin, J. & Sajda, P. Pre-stimulus functional networks modulate task performance in time-pressured evidence gathering and decision-making. *NeuroImage* **111**, 513–525 (2015).
72. Healey, M. K. & Kahana, M. J. A four-component model of age-related memory change. *Psychological Rev.* **123**, 23 (2016).
73. Strange, B. A. & Dolan, R. J. Adaptive anterior hippocampal responses to oddball stimuli. *Hippocampus* **11**, 690–698 (2001).
74. Yebra, M. et al. A gradient of electrophysiological novelty responses along the human hippocampal long axis, bioRxiv (2021) 2021–11.
75. Krebs, R. M., Schott, B. H., Schütze, H. & Düzel, E. The novelty exploration bonus and its attentional modulation. *Neuropsychologia* **47**, 2272–2281 (2009).
76. Lisman, J. E. & Grace, A. A. Pittsburgh, pennsylvania 15260 the role of the hippocampus in producing novelty-dependent firing of vta cells. *Neuron* **46**, 703–713 (2005).
77. Leutgeb, J. K., Leutgeb, S., Moser, M.-B. & Moser, E. I. Pattern separation in the dentate gyrus and ca3 of the hippocampus. *science* **315**, 961–966 (2007).
78. Bakker, A., Kirwan, C. B., Miller, M. & Stark, C. E. Pattern separation in the human hippocampal ca3 and dentate gyrus. *science* **319**, 1640–1642 (2008).
79. Baker, S. et al. The human dentate gyrus plays a necessary role in discriminating new memories. *Curr. Biol.* **26**, 2629–2634 (2016).
80. De Shetler, N. G. & Rissman, J. Dissociable profiles of generalization/discrimination in the human hippocampus during associative retrieval. *Hippocampus* **27**, 115–121 (2017).
81. Lacy, J. W., Yassa, M. A., Stark, S. M., Muftuler, L. T. & Stark, C. E. Distinct pattern separation related transfer functions in human ca3/dentate and ca1 revealed using high-resolution fmri and variable mnemonic similarity. *Learn. Mem.* **18**, 15–18 (2011).
82. Vieweg, P., Stangl, M., Howard, L. R. & Wolbers, T. Changes in pattern completion–a key mechanism to explain age-related recognition memory deficits? *Cortex* **64**, 343–351 (2015).
83. Horner, A. J. & Burgess, N. Pattern completion in multielement event engrams. *Curr. Biol.* **24**, 988–992 (2014).
84. McClelland, J. L. & Goddard, N. H. Considerations arising from a complementary learning systems perspective on hippocampus and neocortex. *Hippocampus* **6**, 654–665 (1996).
85. Knierim, J. J. & Zhang, K. Attractor dynamics of spatially correlated neural activity in the limbic system. *Annu. Rev. Neurosci.* **35**, 267–285 (2012).
86. Rotello, C. M., Macmillan, N. A. & Van Tassel, G. Recall-to-reject in recognition: Evidence from roc curves. *J. Mem. Lang.* **43**, 67–88 (2000).
87. Yonelinas, A., Kroll, N., Dobbins, I. & Soltani, M. Recognition memory for faces: When familiarity supports associative recognition judgments. *Psychonomic Bull. Rev.* **6**, 654–661 (1999).
88. Quamme, J. R., Yonelinas, A. P. & Norman, K. A. Effect of unitization on associative recognition in amnesia. *Hippocampus* **17**, 192–200 (2007).
89. Diana, R. A., Yonelinas, A. P. & Ranganath, C. The effects of unitization on familiarity-based source memory: testing a behavioral prediction derived from neuroimaging data., Journal of Experimental Psychology: Learning, Memory. *Cognition* **34**, 730 (2008).
90. Kumaran, D. & Maguire, E. A. An unexpected sequence of events: mismatch detection in the human hippocampus. *PLoS Biol.* **4**, e424 (2006).
91. Chen, J., Olsen, R. K., Preston, A. R., Glover, G. H. & Wagner, A. D. Associative retrieval processes in the human medial temporal lobe: hippocampal retrieval success and ca1 mismatch detection. *Learn. Mem.* **18**, 523–528 (2011).
92. Kumaran, D. & Maguire, E. A. Match–mismatch processes underlie human hippocampal responses to associative novelty. *J. Neurosci.* **27**, 8517–8524 (2007).

93. Buzsáki, G. Theta rhythm of navigation: link between path integration and landmark navigation, episodic and semantic memory. *Hippocampus* **15**, 827–840 (2005).
94. Greicius, M. D. et al. Regional analysis of hippocampal activation during memory encoding and retrieval: fmri study. *Hippocampus* **13**, 164–174 (2003).
95. Geller, A. S., Schleifer, I. K., Sederberg, P. B., Jacobs, J. & Kahana, M. J. Pyepl: A cross-platform experiment-programming library. *Behav. Res. Methods* **39**, 950–958 (2007).
96. Nelson, D. L., McEvoy, C. L. & Schreiber, T. A. The university of south florida free association, rhyme, and word fragment norms, Behavior Research Methods, Instruments. *Computers* **36**, 402–407 (2004).
97. de Chastelaine, M., Mattson, J. T., Wang, T. H., Donley, B. E. & Rugg, M. D. The relationships between age, associative memory performance, and the neural correlates of successful associative memory encoding. *Neurobiol. Aging* **42**, 163–176 (2016).
98. Hou, M., Horne, E. D., de Chastelaine, M. & Rugg, M. D. Divided attention at retrieval does not influence neural correlates of recollection in young or older adults. *NeuroImage* **250**, 118918 (2022).
99. Kook, H., Gupta, L., Kota, S., Molfese, D. & Lyytinen, H. An offline/real-time artifact rejection strategy to improve the classification of multi-channel evoked potentials. *Pattern Recognit.* **41**, 1985–1996 (2008).
100. Ludbrook, J. Advantages of permutation (randomization) tests in clinical and experimental pharmacology and physiology. *Clin. Exp. Pharmacol. Physiol.* **21**, 673–686 (1994).
101. Bhattacharya, J. & Petsche, H. Phase synchrony analysis of eeg during music perception reveals changes in functional connectivity due to musical expertise. *Signal Process.* **85**, 2161–2177 (2005).
102. Berens, P. Circstat: a matlab toolbox for circular statistics. *J. Stat. Softw.* **31**, 1–21 (2009).
103. Hernandez, J., Carrasco-Ochoa, J. A. & Martínez-Trinidad, J. F. An empirical study of oversampling and undersampling for instance selection methods on imbalance datasets, in: Progress in Pattern Recognition, Image Analysis, Computer Vision, and Applications: 18th Iberoamerican Congress, CIARP 2013, Havana, Cuba, November 20-23, 2013, Proceedings, Part I 18, Springer, 2013, pp. 262–269.
104. Yaffe, R. B. et al. Reinstatement of distributed cortical oscillations occurs with precise spatiotemporal dynamics during successful memory retrieval. *Proc. Natl Acad. Sci.* **111**, 18727–18732 (2014).
105. Staresina, B. P. et al. Hierarchical nesting of slow oscillations, spindles and ripples in the human hippocampus during sleep. *Nat. Neurosci.* **18**, 1679–1686 (2015).
106. To, T. Hippocampal Electrode Data and Models https://doi.org/10.18738/T8/GIZHOK (2024).

Acknowledgements

This work was funded by the National Institute of Neurological Disorders and Stroke-National Institutes of Health (Grant R01 NS107357-02 to B.C.L.).

Author contributions

D.X.W. and B.C.L. designed research question and collected data; D.X.W. and T.V.T. performed the experiment; T.V.T. analyzed data; T.V.T., C.B.W. and B.C.L. reviewed and interpreted the results. T.V.T., C.B.W. and B.C.L. wrote the paper.

Competing interests

The authors declare no competing interests.

Additional information

Supplementary information The online version contains supplementary material available at https://doi.org/10.1038/s41467-025-61464-z.

Correspondence and requests for materials should be addressed to Bradley C. Lega.

Peer review information *Nature Communications* thanks Bryan Strange and the other, anonymous, reviewer(s) for their contribution to the peer review of this work. A peer review file is available.